Coupled-volume multi-scale modelling of quasi-brittle material

I.M. Gitman, H. Askes, L.J. Sluys

Coupled-volume multi-scale modelling of quasi-brittle material

I.M. Gitman, H. Askes, L.J. Sluys

PII: S0997-7538(07)00097-6
DOI: 10.1016/j.euromechsol.2007.10.004
Reference: EJMSOL 2385

To appear in: *European Journal of Mechanics A/Solids*

Received date: 30 March 2007
Revised date: 29 September 2007
Accepted date: 16 October 2007

Please cite this article as: I.M. Gitman, H. Askes, L.J. Sluys, Coupled-volume multi-scale modelling of quasi-brittle material, *European Journal of Mechanics A/Solids* (2007), doi: 10.1016/j.euromechsol.2007.10.004

Coupled-volume multi-scale modelling of quasi-brittle material

I.M. Gitman[1], H. Askes[2] & L.J. Sluys[3]

[1] The University of Manchester, School of Mechanical, Aerospace and Civil Engineering,
P.O. Box 88, Sackville Street, Manchester M60 1QD, United Kingdom,
inna.gitman@manchester.ac.uk

[2] University of Sheffield, Department of Civil and Structural Engineering,
Mappin Street, Sheffield S1 3JD, United Kingdom,
h.askes@sheffield.ac.uk

[3] Delft University of Technology, Faculty of Civil Engineering and Geosciences,
P.O. Box 5048, 2600 GA Delft, Netherlands,
l.j.sluys@citg.tudelft.nl

Abstract

The hierarchical multi-scale procedure is analysed in this paper. A local multi-scale model has been studied with respect to the macro-level mesh size and meso-level cell size dependency. The material behaviour has been analysed in case of linear-elasticity, hardening and softening. Though the results show no dependency in cases of linear-elasticity and hardening, a strong dependency on both macro-level mesh size and meso-level cell size in case of softening has been found. In order to eliminate both macro-level mesh size and meso-level cell size dependency, a new multi-scale procedure has been proposed. This procedure uniquely links the numerical parameter "macro-level mesh size" with the model parameter "meso-level cell size". The results of this *coupled-volume* multi-scale model show no dependency on the macro-level mesh size or meso-level cell size.

Keywords: multi-scale, homogenisation, coupled-volume multi-scale model, local model, non-local model

1 Introduction

A general framework to link material properties at two levels of description, incorporating both physical and geometrical nonlinearities, was suggested in 1984 by Hill [Hill, 1984]. He described the material as heterogeneous on one level, while on the other hand he considered the macroscopic behaviour to be homogeneous. In the 1980s and the 1990s the interest in multi-scale approaches was increasing rapidly, with applications ranging from concrete-like composites [Zimmermann et al., 2003] to polycrystalline materials [Miehe et al., 1999] and porous media [Trukozko and Zijl, 2002]. Since the same material point is considered on two levels of observation simultaneously, this approach is also called *hierarchical*, and in this paper the term *multi-scale* should be understood as being hierarchical.

1.1 Analytical continualisation and homogenisation this Section has been shortened significantly

In order to provide a categorisation of the various strategies that are used in multi-scale analysis, a main distinction is made between those approaches that lead to *closed-form expressions* on the macro-level and those approaches that do not. In the former, analytical techniques are used in combination with continualisation or homogenisation. Analytical multi-scale techniques comprise continualisation and homogenisation. The main difference between the two is the representation of the material on the meso-level: in continualisation techniques the material is modelled on the meso-level

Running title. Coupled-volume multi-scale modelling

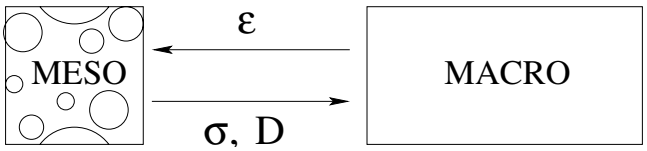

Figure 1: Computational homogenisation

as a discrete medium consisting of masses and springs, e.g., whereas in homogenisation techniques the meso-level material representation is a heterogeneous continuum. Thus, continualisation indicates that a discrete model is translated into a (homogeneous) continuum model, and homogenisation indicates that a heterogeneous continuum is translated into a homogeneous continuum.

Using continualisation techniques, classical and higher-order continua were derived in [Chang and Gao, 1995] and [Mühlhaus and Oka, 1996]. Later, [Suiker et al., 2001] elaborated further upon these works. Random particle packings were considered, by which the constitutive coefficients on the macro-level were obtained as summations over all inter-particle contacts within the considered volume. Isotropy of the resulting macroscopic continuum was addressed in [Askes and Metrikine, 2005]. A continuum model including micro-inertia for heterogeneous materials on the micro-level under dynamic loading was proposed in [Wang and Sun, 2002]. The macro-level strain and stress are defined as the volume averages of the strain and stress fields in the unit cell. Although the conventional definitions of *volume-averaged* stresses and strains are adopted in their formulation, the *local* dynamic equations of motion are used. As a result, the macro strain energy density and the macro kinetic energy density contain the micro-inertia. Consequently, when Hamilton's principle is employed to obtain the macro equations of motion, an effective body force term appears in the macro equations of motion. This effective body force which is absent in the conventional continuum mechanics formulation, contains the micro-inertia effect. Another continualisation procedure was proposed in [Metrikine and Askes, 2002]. The kinematic coupling between the displacements of the discrete model and the continuum was formulated as a weighted average. The obtained continuum description was automatically equipped with micro-inertia as well as higher-order stiffness contributions [Metrikine and Askes, 2002, Askes and Metrikine, 2002].

Similar to continualisation, in analytical homogenisation techniques the macroscopic constitutive relations are obtained in closed form with quantitative information from the meso-level. Analytical homogenisation procedures are an efficient modelling tool for elastic materials. A standard elasticity format was used in [Guedes and Kikuchi, 1990] to determine the effective elastic constants of general composite materials. In [Peerlings and Fleck, 2004] a strain-gradient approach has been proposed to describe the materials behaviour. They determined all elastic constants (classical and higher-order) as effective properties from a number of boundary value problems solved on periodic microstructures. A micromechanical-based approach has also been used by [Fatemi et al., 2003]. They derived the effective Cosserat elastic moduli of cellular solids using analytical homogenisation. They assumed that on the micro-level the "cell wall" material is classically elastic and on the macro-level it behaves as a homogeneous Cosserat-type solid. To derive the effective elastic Cosserat constants, a Cosserat homogenisation technique has been used. Kinematic boundary conditions in terms of displacement and rotation were applied on the representative material sample (RVE). The coefficients of the overall Cosserat elastic tensors for the equivalent homogeneous medium have been determined by relating the resulting Cauchy stress and couple stress tensors (from the response of the material sample) to the applied strain and curvature tensors. More recently, also nonlinear material behaviour has been modelled with analytical homogenisation approaches, see for instance [van der Sluis, 2001]. However, the complexity of the problem increases significantly due to the choices available for the a priori assumed macroscopic constitutive relation. In [Gitman et al., 2005, Gitman et al., 2007a] an analytical homogenisation technique is discussed, that does not rely upon a priori assumptions of the macro-level constitutive relation. However, it must be assumed that local perturbations of stiffness and strain remain small. If higher-order terms are taken into account, this procedure leads to higher-order stiffness terms as well as higher-order inertia terms.

1.2 Computational homogenisation

Instead of analytical continualisation or homogenisation, computational homogenisation (as illustrated in fig. 1) can be used. The difference of this approach from the one discussed above is the absence of an explicitly defined constitutive equation on the macro-level. The macroscopic constitutive relation is implicitly provided by the macro-meso-macro con-

nection. The concept of computational homogenisation can be summarised as follows:

- **macro-level computation:** the material is described as homogeneous with *effective properties* but it does not require any constitutive assumption;
- **down-scaling:** to every integration point of the discretised macro-level a meso-level unit cell is assigned. The macro-level strain field is translated into meso-level displacement boundary conditions;
- **meso-level computations:** the material is described as heterogeneous with a particular composite structure. Each component of the structure has its own constitutive assumption. A boundary value problem is solved for each meso-level unit cell with the boundary conditions as given from the macro-level input. The boundary value problem can be solved in different manners, the most popular being the finite element method ([Smit et al., 1998, Feyel and Chaboche, 2000, Terada and Kikuchi, 2001, Kouznetsova et al., 2001, Miehe et al., 1999]), sometimes in its specific format of the Voronoi cell finite element method ([Lee and Ghosh, 1995, Lee and Ghosh, 1996, Ghosh et al., 2001, Kanit et al., 2003]). Alternatively, Fast Fourier Transforms could be used ([Michel et al., 1999]).
- **up-scaling:** homogenisation is performed on the meso-level response in terms of reaction forces and stiffness relations, which results in the *effective properties* of the homogeneous material to be transfered to the macro-level.

A multi-scale finite element model has been developed in [Lee and Ghosh, 1996] and [Ghosh et al., 2001] for the elastic-plastic analysis of heterogeneous (porous and composite) materials by combining an asymptotic homogenisation theory. Modelling the behaviour of structures reinforced by long fibre SiC/Ti composite materials with a periodic microstructure in [Feyel and Chaboche, 2000] the multi-scale approach has been used in order to take heterogeneities into account in the behaviour between the fibre and matrix.

A multi-scale approach was also applied in biomechanics in order to predict local cell deformations in engineered tissue constructs. For instance, in [Breuls et al., 2002] the compression of a skeletal muscle tissue was analysed to construct and study the influence of microstructural heterogeneity on local cell deformations. Cell deformations are predicted from a detailed nonlinear finite element analysis of the microstructure, consisting of an arrangement of cells embedded in matrix material. Effective macroscopic tissue behaviour is derived by a computational homogenisation procedure. Recently, some advances have been made in the formulation of multi-scale methods. Different homogenisation schemes within a multi-scale approach have been studied extensively in [Kouznetsova, 2002]. Damage evolution in masonry structures has been modelled in [Massart, 2003] with the help of multi-scale modelling framework, in which the equilibrium equations were solved together with a diffusion-type equation on both levels.

The computational homogenisation approach as outlined above bears some similarities with the 'substructuring' technique. In the substructuring technique, the macroscopic domain is split into a number of adjacent but non-overlapping subdomains. The macroscopic boundary value problem is reformulated accordingly. For each subdomain, effective stiffness properties are derived, after which the subdomains are assembled into a macroscopic formulation. The differences with computational homogenisation are

- in computational homogenisation, the unit cell is assigned to a macroscopic integration point, i.e. an infinitely small material point, whereas in substructuring the subdomains are related to finite-size parts of the macroscopic domain;
- computational homogenisation does not require that the individual unit cells are adjacent or non-overlapping;
- in substructuring, the macroscopic effective properties are directly formulated in terms of forces and the corresponding stiffness properties, whereas in computational homogenisation the transition is made from meso-level forces and structural stiffness to macro-level stresses and material stiffness.

The substructuring approach has been applied to multi-scale mechanics by [Zohdi et al., 2001].

Another related approach in the field of multi-scale mechanics is the so-called Arlequin method [Ben Dhia and Rateau, 2005, Ben Dhia, 2006]. In this method, those parts of the domain that require more detailed analysis are modelled as a superposition of a number of numerical models, each of which has a different level of detail. The total energy of the structure is distributed in a weighted manner over the various models. The models can then be joined using Lagrange multipliers or penalty methods. The Arlequin method can be envisaged as a generalisation of computational homogenisation: the energy weights associated with the various numerical models would be unity in computational homogenisation whereas more flexible distributions are possible in the Arlequin method. In the sequel, however, the focus will be restricted to computational homogenisation.

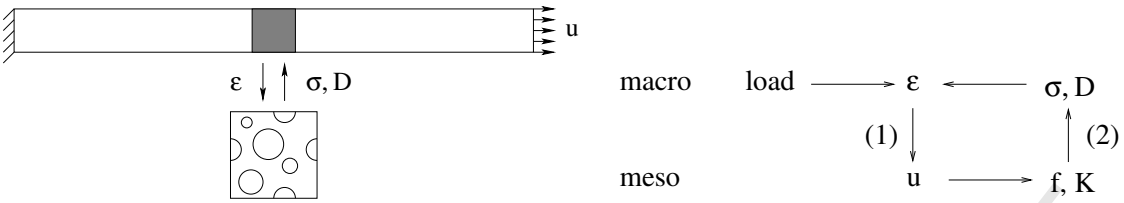

Figure 2: Multi-scale procedure: typical test set-up with down-scaling (1) and up-scaling (2)

2 Multi-scale computational homogenisation algorithm

In this Section the main steps of the computational hierarchical multi-scale procedure are presented. First of all the material is considered on the higher level (macro-level). Then in order to improve the accuracy of the response (in the regions of critical activity) the meso-level is analysed. Finally, the results from the meso-level are transferred back to the macro-level.

The meso-macro connection is used as a constitutive equation on the macro-level. Thus, instead of an explicit formulation of the stress-strain relation, data from the meso-level is considered. The main idea of the hierarchical multi-scale technique is as follows: the strain from the macro-level goes directly in the form of essential boundary conditions to the meso-level, where the material behaviour is simulated (assuming the material to be a heterogeneous continuum), after which the reaction forces to the essential boundary conditions are transformed by means of a homogenisation technique as stresses back to the macro-level. Schematically, the procedure is presented in fig. 2. On the left, a typical test is presented: the one-dimension bar with an imperfection is loaded in tension. A block-scheme of the multi-scale procedure is shown on the right, in which (1) corresponds to the *down-scaling* and transforms the macroscopic strain value into the displacement boundary condition at meso-level; (2) represents the *up-scaling* mechanism, through computational homogenisation. The sequential steps in the multi-scale scheme as mentioned in fig. 2 will be discussed next.

Macro-level: on the macro-level the material is assumed to have a homogeneous structure, so the properties of the material are averaged. The mechanical loading is applied at macro-level and it should be in equilibrium with the internal forces which are computed from the stresses, which are computed at meso-level.

Macro-meso connection: the macroscopic strain field is translated into essential boundary conditions in terms of the vertex displacements of the meso-level cell in the following way:

$$u_x^1 = 0 \qquad u_y^1 = 0 \tag{1a}$$

$$u_x^2 = \varepsilon_{xx}^M L_x^m \qquad u_y^2 = \frac{1}{2}\gamma_{xy}^M L_x^m \tag{1b}$$

$$u_x^3 = \frac{1}{2}\gamma_{xy}^M L_x^m + \varepsilon_{xx}^M L_x^m \qquad u_y^3 = \frac{1}{2}\gamma_{xy}^M L_y^m + \varepsilon_{yy}^M L_y^m \tag{1c}$$

$$u_x^4 = \frac{1}{2}\gamma_{xy}^M L_y^m \qquad u_y^4 = \varepsilon_{yy}^M L_y^m \tag{1d}$$

where ε_{xx}^M, ε_{yy}^M and γ_{xy}^M are macro-level strain components, L_x^m and L_y^m are horizontal and vertical dimensions of the meso-level cell, u is the meso-level displacement with bottom indices showing the corresponding degree of freedom and top indices representing the corner node number – here the numbering starts from the bottom left vertex and proceeds anti-clockwise. Periodic boundary conditions are imposed on the displacements such that the displacements of left and right edge, as well as of top and bottom edge, are identical apart from the macroscopic stretch given through eq. (1). Accordingly, the tractions on opposite edges are of equal magnitude but of opposite sign.

Note 1 *Not only periodic boundary conditions are used, but in the modelling of the mesostructure also periodicity of the material is assumed — see for instance fig. 3 in where particles penetrating the bottom edge re-enter through the top edge.*

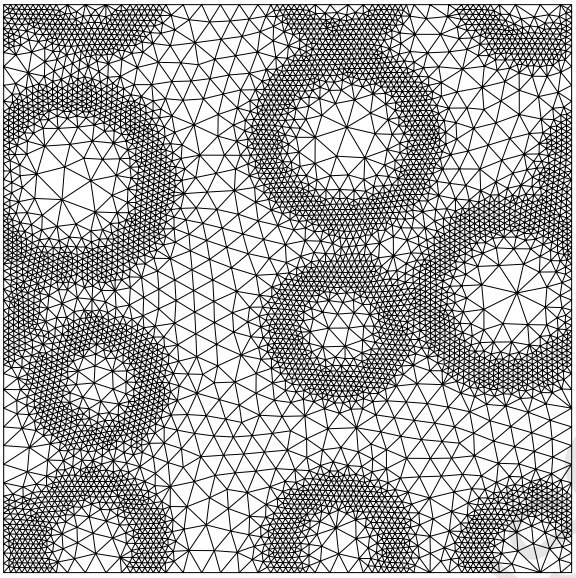

Figure 3: Meso-level unit cell

Materials components properties	Inclusions	Matrix	ITZ
Young's modulus E [MPa]	30000	25000	20000
Poisson's ratio ν [-]	0.2	0.2	0.2

Table 1: Material components properties

Abandoning either periodicity of material or periodicity of boundary conditions will lead to larger sizes of the required meso-level cell, which can strongly influence the results of the multi-scale computation [Gitman et al., 2006, Gitman et al., 2007b].

Meso-level: at meso-level a heterogeneous material is considered; here a three-phase material is investigated. The first phase consists of inclusions (stiff); the second phase is the matrix (less stiff) and the third phase is the interfacial transition zone between inclusions and matrix (least stiff zone). Each of these phases has its own properties (E – Young's modulus, ν – Poisson's ratio etc. cf. tab. 1). The cracking mechanism in the meso-level is caused by mechanical loading only.

Note 2 *The material with the above properties could be the representation of a concrete (Young's modulus and Poisson's ratio were chosen in this paper as corresponding to a concrete), but generally, any three phase composite material (or even two phase material with two out of three phases bearing the same properties) could be described.*

An elasticity-based gradient damage model ([Lemaitre and Chaboche, 1990, Peerlings, 1999, Simone, 2003]) in its implicit formulation is used for the materials component description.

$$\sigma = (1-\omega)D : \varepsilon \tag{2}$$

$$\bar{\varepsilon} - c\nabla^2\bar{\varepsilon} = \tilde{\varepsilon} \tag{3}$$

where σ and ε are stresses and strains, respectively, D is the matrix of elastic stiffness and ω is a damage parameter, $\bar{\varepsilon}$ represents non-local strain. The coefficient c represents here the internal length scale of the non-local model, it has the dimension of length squared: for example for the Gaussian weight function ([Peerlings, 1999]) $c = \frac{1}{2}\ell^2$, with ℓ being related to the scale of the microstructure. The damage grow is controlled by the damage loading function

$$f(\tilde{\varepsilon}, \kappa) = \tilde{\varepsilon} - \kappa \tag{4}$$

Here κ is a history-dependent parameter and $\tilde{\varepsilon}$ is a local equivalent strain following, here, Mazars criterion

$$\tilde{\varepsilon} = \sqrt{\sum_{i=1}^{3} (<\varepsilon_i>)^2} \tag{5}$$

with ε_i the principal strains and $<\varepsilon_i>=\varepsilon_i$ if $\varepsilon > 0$ and $<\varepsilon_i>=0$ otherwise. The damage history of the material is described by the history-dependent parameter κ which is by definition increasing during the loading with non-negative rate. The damage grows is possible if $\dot{\kappa} > 0$. The evolution of this parameter follows the Kuhn-Tucker conditions:

$$\dot{\kappa} \geq 0, \quad f(\tilde{\varepsilon}, \kappa) \leq 0, \quad \dot{\kappa} f(\tilde{\varepsilon}, \kappa) = 0. \tag{6}$$

The damage parameter ω is described as a function of the history-dependent parameter κ: $\omega = \omega(\kappa)$. The exponential softening law is employed here as an evolution law:

$$\omega = \begin{cases} 0 & \text{if} \quad \kappa < \kappa_0 \\ 1 - \frac{\kappa_0}{\kappa}(1 - \alpha + \alpha \exp(-\beta(\kappa - \kappa_0))) & \text{if} \quad \kappa \geq \kappa_0 \end{cases} \tag{7}$$

model parameters α and β represent the residual stress level and the slope of the softening curve, respectively.

The crack initiation strains and length-scale parameters (which provides the link with the underlying micro-structure, and, here, for simplicity, chosen to be equal for all three phases) are specified in tab. 2. The crack initiation strain of the

Materials components properties	Inclusions	Matrix	ITZ
Crack initiation strain κ_0 [-]	0.5	5.0e-06	3.0e-06
Length-scale parameter ℓ [mm]	0.63	0.63	0.63
Residual stress parameter α [-]	0.999	0.999	0.999
Slope of softening β [-]	1500	1500	1500

Table 2: Material components properties

inclusions has been chosen artificially high in order to avoid crack propagation through the inclusions.

The essential boundary conditions are given in eqs. (1) with the periodic boundary conditions linking both displacement components of opposite edges. Again, fracture at the meso-level can take place in the cement paste or in the interfacial transition zone (ITZ).

Meso-macro connection: the stresses and tangent moduli at macro-level are computed from their associated quantities at meso-level. Thus, instead of an *explicit* formulation of the macro-level constitutive equation, information from the meso-level is used. In order to keep the meso-macro relation consistent, and bearing in mind the homogeneous description of the material at macro-level and heterogeneous material definition at meso-level, the procedure of homogenisation should be carried out.

The average value of stresses in the meso-level can be computed via

$$<\sigma^{\mathrm{m}}> = \frac{1}{V_{\mathrm{m}}} \int_{\Omega} \sigma^{\mathrm{m}} dV \tag{8}$$

The average value of the stress in the meso-level $<\sigma^{\mathrm{m}}>$ is equal to the value of the stress in the macro-level σ^{M} in the considered integration point at macro-level (eq. (9)):

$$\sigma^{\mathrm{M}} = <\sigma^{\mathrm{m}}> \tag{9}$$

In order to obtain the macro-level stiffness matrix the following steps are performed:

- Firstly, the meso-level stiffness matrix is partitioned as

$$\begin{bmatrix} K_{ff} & K_{fp} \\ K_{pf} & K_{pp} \end{bmatrix} \begin{bmatrix} \delta u_f \\ \delta u_p \end{bmatrix} = \begin{bmatrix} 0 \\ \delta f_p \end{bmatrix} \tag{10}$$

  Here δu_p and δf_p correspond to the values of iterative displacements and residual forces of the *prescribed* nodes, respectively, i.e. the four corner nodes of the meso-level; δu_f consists of the iterative displacements of the *free* nodes (the rest of the nodes in the discretised meso-level). Furthermore, for a converged solution $\delta f_f = 0$.

- Eq. (10) can then be rewritten as

$$K^{\mathrm{M}} \cdot \delta u_p = \delta f_p \tag{11}$$

where

$$K^{\mathrm{M}} = K_{pp} - K_{pf} K_{ff}^{-1} K_{fp} \tag{12}$$

Thus, for the prescribed boundary nodes it can be written that

$$\sum_j K_{ij}^{\mathrm{M}} \cdot \delta u_p^j = \delta f_p^i \tag{13}$$

with i and j being the degrees of freedom of the corner nodes

- Next, an expression for the stresses is written as

$$\delta\sigma^{\mathrm{M}} = \frac{1}{V_{\mathrm{m}}} \sum_i \delta f_p^i \mathbf{x}^i = \frac{1}{V_{\mathrm{m}}} \sum_i \sum_j (K_{ij}^{\mathrm{M}} \cdot \delta u_p^j) \mathbf{x}^i \tag{14}$$

Bearing in mind that $\delta u_p^j = \mathbf{x}^j \cdot \delta\varepsilon^{\mathrm{M}}$ it is possible to rewrite the stresses as

$$\delta\sigma^{\mathrm{M}} = \frac{1}{V_{\mathrm{m}}} \sum_i \sum_j (K_{ij}^{\mathrm{M}} \cdot \mathbf{x}^j \cdot \delta\varepsilon^{\mathrm{M}}) \mathbf{x}^i = \frac{1}{V_{\mathrm{m}}} \sum_i \sum_j (\mathbf{x}^i K_{ij}^{\mathrm{M}} \mathbf{x}^j)^{\mathrm{C}} : \delta\varepsilon^{\mathrm{M}} \tag{15}$$

- Thus, the macro-level constitutive tangent stiffness D^{M} on the meso-level can be presented as

$$D^{\mathrm{M}} = \frac{1}{V_{\mathrm{m}}} \sum_i \sum_j \mathbf{x}^i K_{ij}^{\mathrm{M}} \mathbf{x}^j \tag{16}$$

Note that here $\mathbf{x}^i = (x^i, y^i)$ is the position vector of node i.

With values of stresses and stiffnesses in each macro-level integration point the analysis of the macro-level is continued.

Note 3 *The values of stress and stiffness following the above procedures are computed only after the meso-level finite element calculation has converged.*

Note 4 *The macroscopic stresses can be found from equations (8-9), or by translating the reaction forces to the prescribed displacements given in (1) in a similar way as K^M is translated into D^M.*

The key issue in this multi-scale procedure is the size of the meso-level.

Macrohomogeneity principle. The meso-macro transition should satisfy the macrohomogeneity condition, known also as the Hill-Mandel condition [Hill, 1963, Hill, 1967, Kouznetsova, 2002]. Following Hill's procedure the energy density

$$2U = \sigma_{ij}^{\mathrm{M}} \varepsilon_{ij}^{\mathrm{M}} \tag{17}$$

should then fulfill

$$\sigma_{ij}^{\mathrm{M}} \varepsilon_{ij}^{\mathrm{M}} = \frac{1}{V_{\mathrm{m}}} \int_{\Omega} \sigma_{ij}^{\mathrm{m}} \varepsilon_{ij}^{\mathrm{m}} \mathrm{d}V \tag{18}$$

In order to evaluate eq. (18), let us consider first the right-hand-side:

$$\frac{1}{V_{\mathrm{m}}} \int_{\Omega} \sigma_{ij}^{\mathrm{m}} \varepsilon_{ij}^{\mathrm{m}} \mathrm{d}V = \frac{1}{V_{\mathrm{m}}} \int_{\Omega} \sigma_{ij}^{\mathrm{m}} \nabla_i^s u_j \mathrm{d}V \tag{19}$$

Here the relation between strain and displacement has been used: $\varepsilon_{ij} = \nabla_i^s u_j$. It can be written that

$$\sigma_{ij}^{\mathrm{m}} \nabla_i^s u_j = \nabla_i^s (\sigma_{ij}^{\mathrm{m}} u_j) - (\nabla_i^s \sigma_{ij}^{\mathrm{m}}) u_j \tag{20}$$

where the second term on the right-hand-side vanishes as a result of the meso-level equilibrium. It is now possible to rewrite eq. (19)

$$\frac{1}{V_{\mathrm{m}}} \int_{\Omega} \sigma_{ij}^{\mathrm{m}} \nabla_i^s u_j \mathrm{d}V = \frac{1}{V_{\mathrm{m}}} \int_{\Omega} \nabla_i^s (\sigma_{ij}^{\mathrm{m}} u_j) \mathrm{d}V = \frac{1}{V_{\mathrm{m}}} \int_{\Gamma} f_j u_j \mathrm{d}S \tag{21}$$

Note, that the Gauss divergence theorem has been used as well as $f_j = n_i \sigma_{ij}$. As it has been mentioned above, periodic boundary conditions have been used. As such eq. (21) can be elaborated as

$$\begin{aligned} &\frac{1}{V_{\mathrm{m}}} \int_{\Gamma} f_j u_j \mathrm{d}S = \frac{1}{V_{\mathrm{m}}} \int_{\Gamma^{TR}} f_j^{TR} u_j^{TR} \mathrm{d}S + \frac{1}{V_{\mathrm{m}}} \int_{\Gamma^{BL}} f_j^{BL} u_j^{BL} \mathrm{d}S = \\ &\frac{1}{V_{\mathrm{m}}} \int_{\Gamma} f_j^{TR} (u_j^{TR} - u_j^{BL}) \mathrm{d}S = \frac{1}{V_{\mathrm{m}}} \int_{\Gamma} f_j^{TR} (x_i^{TR} - x_i^{BL}) \mathrm{d}S \varepsilon_{ij}^{\mathrm{M}} = \\ &\frac{1}{V_{\mathrm{m}}} \int_{\Gamma} f_j x_i \mathrm{d}S \varepsilon_{ij}^{\mathrm{M}} \end{aligned} \tag{22}$$

Considering eqs. (8) and (9)

$$\sigma_{ij}^{\mathrm{M}} = \frac{1}{V_{\mathrm{m}}} \int_{\Omega} \sigma_{ij}^{\mathrm{m}} \mathrm{d}V \tag{23}$$

and using the meso-level equilibrium condition $\nabla_k \sigma_{kj}^{\mathrm{m}} = 0$ and the equality to $\nabla_k^s x_i = \delta_{ki}$, it is possible to write

$$\sigma_{ij}^{\mathrm{m}} = (\nabla_k^s \sigma_{kj}^{\mathrm{m}}) x_i + \sigma_{kj}^{\mathrm{m}} (\nabla_k^s x_i) = \nabla_k^s (\sigma_{kj}^{\mathrm{m}} x_i) \tag{24}$$

Substitution of eq. (24) into eq. (23) and applying the Gauss divergence theorem leads to

$$\frac{1}{V_{\mathrm{m}}} \int_{\Omega} \sigma_{ij}^{\mathrm{m}} \mathrm{d}V = \frac{1}{V_{\mathrm{m}}} \int_{\Omega} \nabla_k^s (\sigma_{kj}^{\mathrm{m}} x_i) \mathrm{d}V = \frac{1}{V_{\mathrm{m}}} \int_{\Gamma} f_j x_i \mathrm{d}S = \frac{1}{V_{\mathrm{m}}} \int_{\Gamma} f_j x_i \mathrm{d}S \tag{25}$$

With relation (25), eq. (22) can now be elaborated as

$$\frac{1}{V_{\mathrm{m}}} \int_{\Gamma} f_j x_i \mathrm{d}S \varepsilon_{ij}^{\mathrm{M}} = \sigma_{ij}^{\mathrm{M}} \varepsilon_{ij}^{\mathrm{M}} \tag{26}$$

Thus the macrohomogeneity condition (18) is satisfied.

3 Local multi-scale modelling

First, local multi-scale modelling will be treated. Here, by means of *local* model it will be assumed that only local values of strain, stress and stiffness are considered in the integration point at the macro-level. At the macro-level the material is assumed to be homogeneous. The mechanical loading is applied at the macro-level and it should be in equilibrium with the internal forces which are computed from the stresses at the meso-level. Such a scheme is also known as a first-order homogenisation scheme [Kouznetsova et al., 2002, Gitman et al., 2005].

As an illustration of the multi-scale procedure, a tension bar as shown in fig. 2 is analysed. On the macro-level, a one-dimensional bar with length $L = 600$ mm and cross-sectional area $A = 1$ mm^2 is considered. The material is considered to be homogeneous with an imperfection in the middle of the macro-structure (10% reduction in cross-section). The macro-level is discretised by means of linear one-dimensional elements with one integration point per element. Every macroscopic integration point of the discretised bar has an equivalent on the meso-level. On the meso-level, the material is considered to be heterogeneous: matrix with inclusions, surrounded by an interfacial transition zone. Each of these components has its own mechanical properties. Periodic boundary conditions together with material periodicity [Gitman,

2006] are used on the meso-level. At meso-level material parameters were chosen as presented in tabs. 1–2. Note again, that the crack initiation strain of the inclusions has been chosen artificially high in order to avoid the crack propagation through the inclusions and the length-scale parameters, for simplicity, have been chosen to be equal for all three phases. The size of the meso-level elements have been chosen accordingly to the length-scale parameter: the matrix element size has been taken as 3 time as small as the length-scale parameter. The size of the ITZ elements was chosen smaller than the size of the matrix elements in order to capture the curvature of the crack in the neighbourhood of an inclusion. The size of the elements in inclusions has been taken much larger in order to save computer time.

In order to be able to follow the solution into regimes of snap-back (when it appears) at macro-level the arc-length control procedure, or more specifically, the indirect displacement control method ([de Borst, 1987]) is employed.

Note 5 *Snap-back behaviour is expected because localisation of deformation in the meso-structure occurs. However, it is emphasized that in the analyses presented here snap-backs appear on the macro-level, not on the meso-level. Taking larger meso-level cells would lead to snap-back behaviour on the meso-level, but this leads to ambiguities in the homogenised stress-strain relation.*

Note 6 *Indirect displacement control is not the only possible choice to control snap-back behaviour. [Massart, 2003] has offered an alternative procedure, the idea of which is to introduce the non-local degree of freedom $\bar{\varepsilon}$ on the meso-level via the implicit gradient damage formulation and define the conjugate residual $f_{\bar{\varepsilon}}$. Adding the condition of $f_{\bar{\varepsilon}} = 0$, satisfying only upon macroscopic convergence, helps controlling the snap-back behaviour. Another possible procedure to control snap-back behaviour has been introduced by [Gutiérrez, 2004]. The method is based on the energy released during failure. The idea of the approach, derived from the first principle of thermodynamics, is to introduce a new interpretation of the path following parameter. This parameter has to be related to a certain monotonically increasing variable, and as such dissipated energy satisfies this requirement in a natural way.*

The results of the multi-scale procedure are analysed in three regimes: linear-elasticity, hardening and softening. In all three of those regimes the issues of meso-level size dependence and macro-level mesh dependence are studied. Following the concept of the RVE, it is known, that with increasing size, the structural behaviour should not be affected. In other words, it should be verified whether the macroscopic response converges with increasing RVE size. On the other hand, a proper reliable model should not be affected by changes in finite element discretisation, i.e. the model should be mesh independent. These both issues have been studied in the framework of the multi-scale model. The response of the material is analysed in terms of the reaction forces on the macro-level for a given imposed displacement.

Subsequently, the sensitivity of the results to the macro-level discretisation and meso-level size has been analysed.

Macro-level mesh dependence. The first issue to analyse is the macro-level mesh dependence. Four different meshes (tab. 3) have been used in order to discretise the macro-level. Note, that the size of the imperfection on the macro-level scales with macro-element size. All macro-meshes have been combined with meso-level cell sizes of $10 \times 10\text{mm}^2$, $15 \times 15\text{mm}^2$, $20 \times 20\text{mm}^2$ and $25 \times 25\text{mm}^2$. Results of the multi-scale procedure for different meshes on the macro-level

MACRO M24	macro-level mesh 24 elements
MACRO M30	macro-level mesh 30 elements
MACRO M40	macro-level mesh 40 elements
MACRO M60	macro-level mesh 60 elements

Table 3: Macro-level meshes

are presented in fig. 4. Based on these results, the following observations can be made:

- in the **pre-peak** regime, according to fig. 4, the material does not show macro-level mesh sensitivity;
- on the contrary, in the **post-peak** or **softening** regime the material experiences mesh dependence: the brittleness is increasing with refining the mesh. Material even can exhibit a *snap-back* behaviour with increasing the number of elements: compare for example the macroscopic responses in cases of mesh M24 and mesh M60 in figs. 4–top-left. In figs. 4–top-right, bottom-left, bottom-right the snap-back behaviour is present for all macro-mesh densities and it is progressing with refining the mesh. Thus, in the softening regime the mechanical behaviour of the material

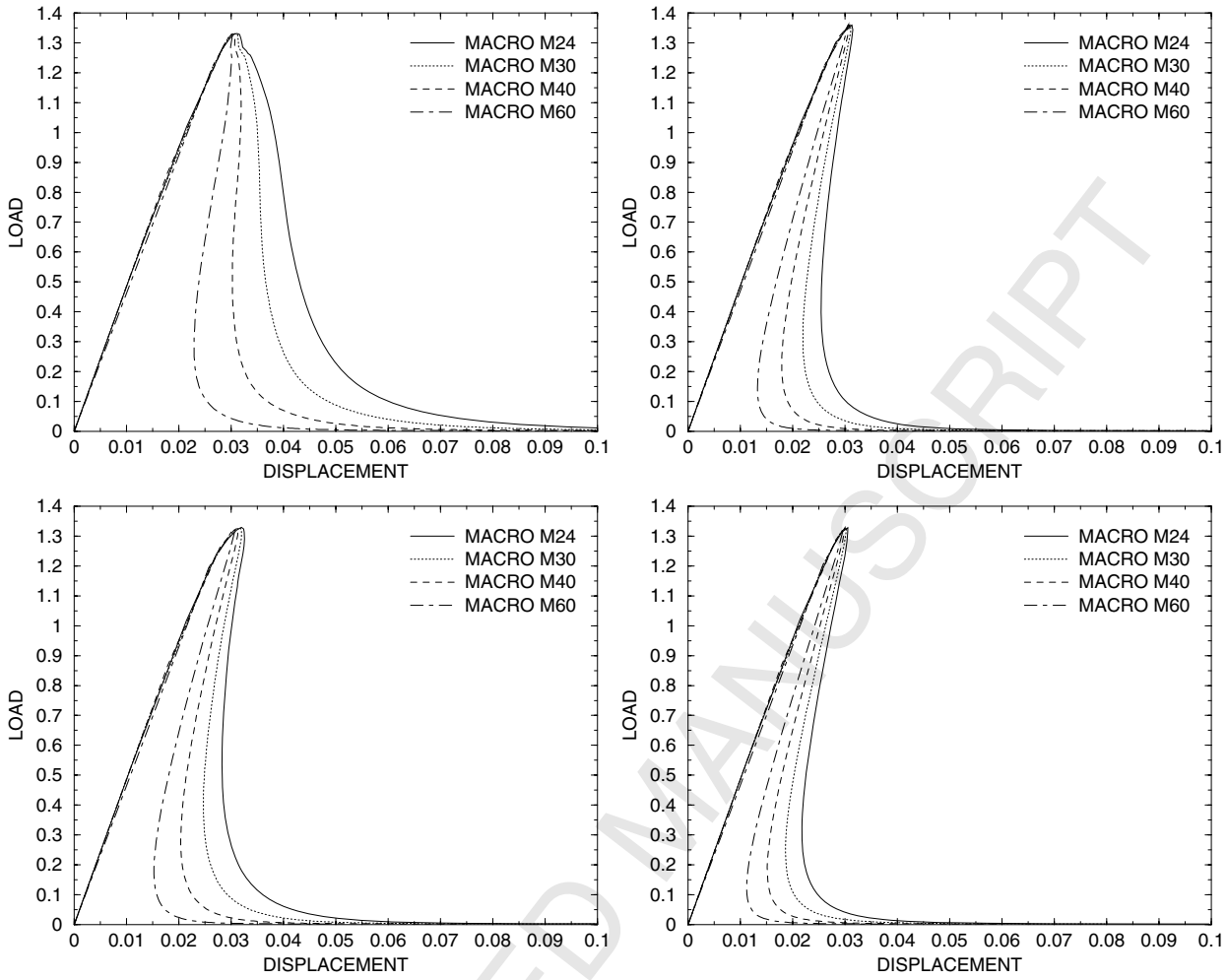

Figure 4: Macro-level mesh dependence (volume fraction of inclusions 45%); meso-level size $10 \times 10\text{mm}^2$ (top left), meso-level size $15 \times 15\text{mm}^2$ (top right), meso-level size $20 \times 20\text{mm}^2$ (bottom left), meso-level size $25 \times 25\text{mm}^2$ (bottom right).

MESO S10	meso-level size 10mm $\times$ 10mm
MESO S15	meso-level size 15mm $\times$ 15mm
MESO S20	meso-level size 20mm $\times$ 20mm
MESO S25	meso-level size 25mm $\times$ 25mm

Table 4: Meso-level sizes

is influenced by the discretisation scheme, irrespective of the meso-level cell size. The fact that the meso-level response is regularised by a length-scale parameter of the gradient damage model does not solve the problem.

Meso-level size dependence. In order to analyse meso-level size dependence, the sizes $10 \times 10\text{mm}^2$, $15 \times 15\text{mm}^2$, $20 \times 20\text{mm}^2$ and $25 \times 25\text{mm}^2$ (tab. 4) have been used for the meso-level. In combination, all four mesh densities MACRO M24 – MACRO M60 have been applied. The results are presented in fig. 5. The following observations can be made:

- in the **pre-peak** regime the material is not sensitive to the changes in the meso-cell size.

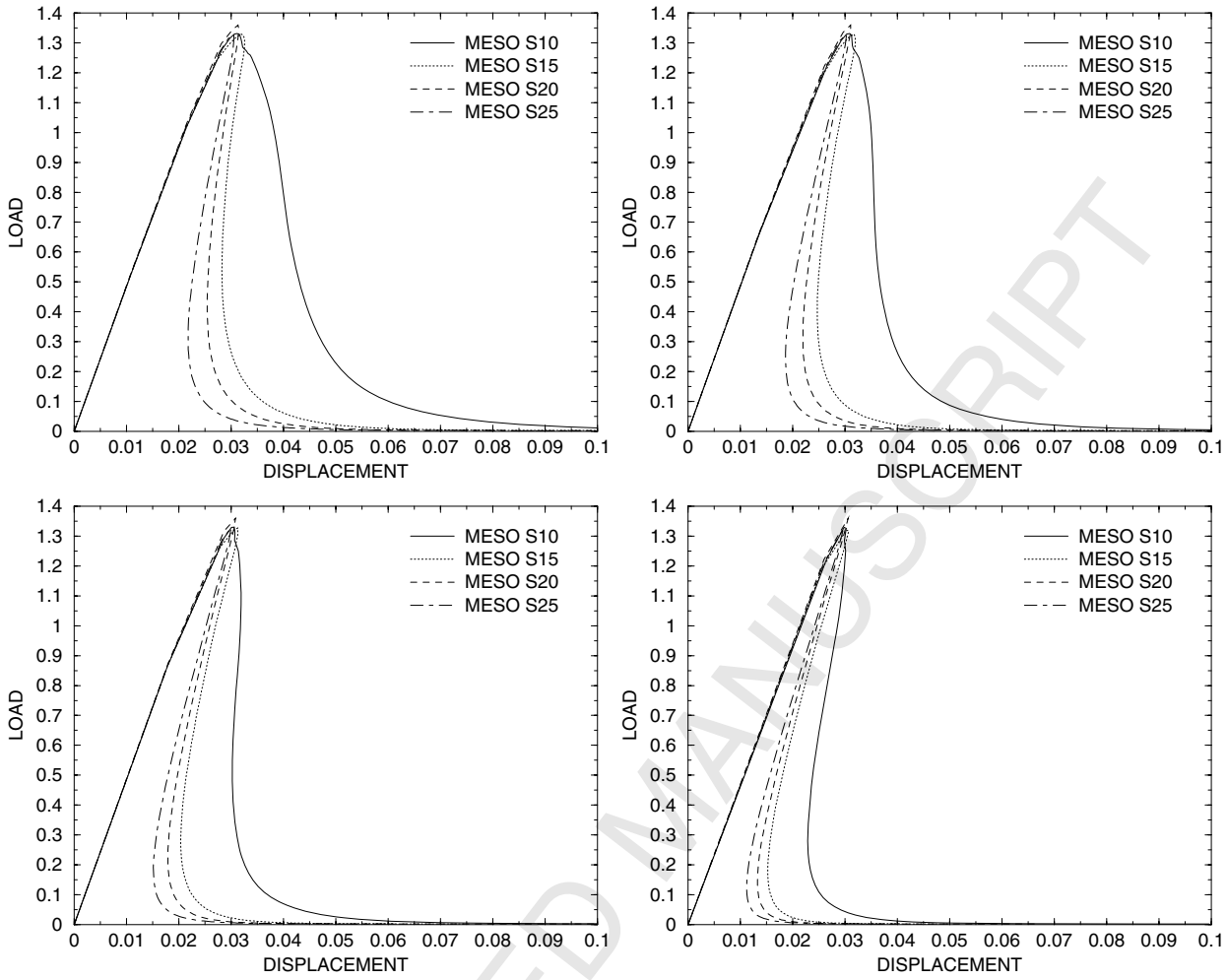

Figure 5: Meso-level size dependence (volume fraction of inclusions 45%); macro-level mesh M24 (top left), macro-level mesh M30 (top right), macro-level mesh M40 (bottom left), macro-level mesh M60 (bottom right).

- However, in the post-peak or **softening** regime increasing the size of the meso-level leads to a more brittle material behaviour. This holds for all macro-level mesh densities. The appearance (fig. 5-top) or increasing (fig. 5-bottom) of snap-back behaviour is again possible as a result of increasing the meso-level size. The big difference between MESO S10 and others (fig. 5) can be explained by the choice of the particular realisation. By increasing the size the difference between the realisations becomes smaller, however the average response still does not converge.

In the pre-peak regime, material is not sensitive to changes in the macro-level mesh and meso-level size. On the contrary, in the softening regime the mechanical behaviour of the material is highly influenced by the discretisation scheme and by the size of the meso-level. The results appear to be in good agreement with the behaviour of the RVE analysed in [Gitman, 2006, Gitman et al., 2007c]: in linear elasticity and hardening the RVE size can be found and it has a unique lower bound, increasing the sample size would not lead to different results. Conversely, in a material with localised deformations the unique size of the RVE cannot be found, thus increasing the sample size would lead to different results.

4 Non–local multi-scale modeling

In the previous Section, the local approach has been analysed: in each integration point of the macro-level the local strain is transferred into meso-level input, and in return the values of the homogenised meso-level stress and stiffness are transferred into a macro-level local stress and stiffness. Despite the fact that the underlying meso-structure of the material is taken into account, this local multi-scale approach suffers from both macro-level mesh dependence and meso-level size dependence. It is noted once again that the meso-level analyses are not mesh dependent because of the higher-order gradient model that is used. One of the ways to overcome these problems could be to introduce *nonlocality* in the multi-scale model. Two major types of non-local models will be discussed here: an integral model and a differential formulation.

Initially introduced to include mesostructural effects and to solve the issue of the discretisation sensitivity, two non-local approaches can be distinguished:

- integral models [Bažant and Pijaudier-Cabot, 1989, Bažant, 1991, Bažant and Jirásek, 1994, Pijaudier-Cabot and Bažant, 1987, Pijaudier-Cabot, 1995], where a non-local strain is introduced as

$$\bar{\varepsilon} = \frac{\int\limits_S \psi(s)\varepsilon(x+s)\mathrm{d}S}{\int\limits_S \psi(s)\mathrm{d}S} \tag{27}$$

  in which $\psi(s)$ is the exponential weight function:

$$\psi(s) = \exp\left(-\frac{s^2}{2\ell^2}\right) \tag{28}$$

  and ℓ is a length-scale parameter

- differential models, where higher-order gradients are included in the constitutive relation. This can be done directly in the stress-strain relation [Ru and Aifantis, 1993] or in the nonlinear evolution laws of the state variables [Peerlings, 1999, Simone, 2003]. This has inspired the development of numerical second-order homogenisation schemes [Kouznetsova, 2002, Kouznetsova et al., 2002], whereby not only the macroscopic strain but also its gradient is used to generate the meso-level boundary value problem. The conjugated variables are then the usual stress but also a higher-order stress, which are extracted from the meso-level together with the appropriate tangent stiffness tensors. The inclusion of strain gradients and higher-order stresses automatically results in the occurrence of a length-scale parameter in the macroscopic response.

Not all of the various formats of the above models are suitable for implementation within a computational homogenisation scheme. For instance, a model should not employ both local strains and nonlocal strains within the same macroscopic equation, since only one strain tensor can be used in the down-scaling procedure.

It has been shown that the second-order homogenisation scheme is linked one-to-one to the differential model as mentioned above [Kouznetsova, 2002]. Indeed, the second-order homogenisation scheme overcomes dependence on the macro-level discretisation. However, this scheme suffers from two disadvantages:

- implementation of the second-order homogenisation scheme is considerably more involved than the first-order homogenisation scheme. Apart from the additional strain gradient and the additional higher-order stress, also three additional tangent stiffness tensors must be evaluated;

- more importantly, the second-order homogenisation scheme does not solve the meso-level size dependence in case of a softening response. Although the RVE ceases to exist in softening, the macroscopic length-scale in a second-order scheme is still proportional to the size of the meso-level sample [Gitman et al., 2005, Gitman et al., 2007a].

Obviously, a conceptually different approach is needed, which could resolve the macro-level discretisation sensitivity and the meso-level size dependency simultaneously.

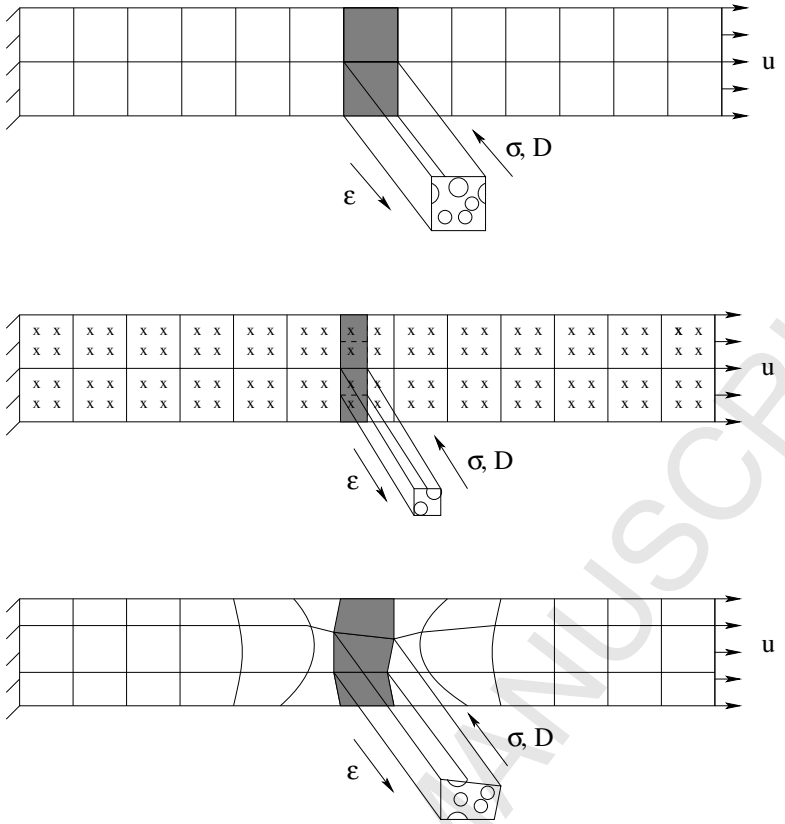

Figure 6: Coupled-volume multi-scale approach: two-dimensional case (top), more than one integration point per element (middle) and elements with arbitrary shape (bottom)

5 Coupled–Volume approach: an alternative multi-scale scheme

The present philosophy of the multi-scale material description has been formulated in [Nemat-Nasser and Hori, 1999], in which the *scales separation principle* sets the interaction between an infinitesimal macro-material point and a finite meso-material volume. However, once localisation occurs on the meso-level, the RVE for such a material can not be found [Gitman, 2006, Gitman et al., 2007c]. Thus the statistically representative meso-material volume does not exist any more; there is no longer a corresponding infinitesimal macro-material point; the *separation of scales* principle is no longer valid. In other words, the decoupling of a macro-level integration point and a meso-level volume is no longer admissible.

An alternative multi-scale model is introduced in this paper. The main idea of this model and the main difference compared with the known multi-scale models is to abandon the idea that a finite meso-level cell size can be linked to an infinitely small macro-level material point. In contrast, the macro-level mesh and meso-level size are uniquely linked. This link, in terms of the given macro-level meshes and meso-level sizes, follows the rule that the macro-level element size *equals* the meso-level cell size. We introduce this approach as the *Coupled-Volume* approach. The attempt to connect model parameters and material parameters has already been made in [Gitman et al., 2005, Gitman et al., 2007a], where the material length-scale has been found in terms of the model parameter RVE size. Here the connection is made between a model parameter (size of the meso-level) and a numerical parameter (size of the macro-level mesh element).

In the current formulation of the coupled-volume approach the one-dimensional case is studied. When comparing different meso-level sample sizes, the height of these samples will change. This change in height can be accounted for on the macro-level by adjusting the cross-sectional area that is used within the one-dimensional problem statement on the macro-level. However, the approach can be extended to two- and three-dimensions. In fig. 6–top the two-dimensional case is presented. In the present case only one integration point per element is allowed. In the case when two or more integration points per element are used the formulation of the method changes and instead of the element size on the

macro-level, the integration volume, i.e. the volume belonging to one integration point, is linked to the meso-level size. This situation is presented in fig. 6–middle. Here, it is noted that the imperfection is concentrated only in one integration point.

The coupled-volume approach may also be extended to the case of arbitrary shaped macro-level elements. The difficulty here would be in constructing the meso-level sample identical to the element on the macro-level (fig. 6–bottom). Once this is done, the assumption of periodicity of boundary conditions on the meso-level can not hold any longer. The following alternatives exist:

- Instead of the periodic boundary conditions, essential boundary condition in the form of displacement on the meso-level can be used: $u_i^{\mathrm{m}} = \varepsilon^{\mathrm{M}} x_i$ where u_i^{m} is the displacement of the boundary node i of the discretised meso-level, ε^{M} is the strain coming from the macro-level and x_i is the position of the node i. However, it is known that such boundary conditions overestimate the stiffness of the meso-level sample significantly [van der Sluis, 2001]. Furthermore, the boundary nodes would then be submitted to a *homogeneous* tangential strain along the edge, which may hamper the propagation of the localised damage zone onto the edge or beyond into a neighbouring meso-level cell;
- Alternatively, the substructuring method mentioned in the Introduction can be used, hereby linking the boundary nodal displacements of adjacent cells. Not only would this preserve the total volume of the specimen during the transition from one scale to the other, but it also provides a framework with which to model crack propagation that is continuous across adjacent cells.

Somewhat similar strategies of coupling meso (micro) and macro scales of observations have been independently reported in [Markovic and Ibrahimbegovic, 2004] and [Massart, 2003]. Both approaches are based on abandoning the separation of scales principle and have addressed the problem of coupling a *periodic* micro-structure to a macro-structure. In contrast to the above works, in the present study random material has been used on the meso-level. Since randomly structured material is considered on the meso-level also the cases of different volume fractions of inclusions are investigated. As it will be discussed below, the statistical study of different meso-level sizes and its influence on the overall response is carried out. The coupled–volume approach is applicable for the case of softening, as will be demonstrated.

5.1 Coupled-volume approach versus fracture-energy-based approach

In this section the coupled-volume multi-scale approach is viewed in connection to the fracture-energy-based approach [Bažant and Oh, 1983]. The idea of the fracture-energy-based approach can be presented by means of the following characteristics:

- as a consequence of the local damage model, results in terms of stress-strain relation show sensitivity to the discretisation, i.e. mesh dependency – the finer the mesh the more brittle material behaves;
- by introducing a material parameter – the fracture energy i.e. the energy that is needed to create a unit area of a fully developed crack – as the area under the stress-displacement diagram, the softening modulus appears to be dependent on the size of the element;
- this results in the dependence of the constitutive behaviour on the element size: the smaller the element size the less brittle the material is
- as a conclusion the two above effects compensate each other, and the fracture energy model is mesh-objective in terms of dissipated energy.

Similar effects can be observed in the coupled-volume approach:

- on one hand, while considering different discretisations on the macro-level and keeping sizes of the meso-level constant, the effect of macro-level mesh dependency can be observed: the finer the mesh, the more brittle the macro-level response (see fig. 4);
- on the other hand, while keeping the discretisation on the macro-level constant and changing the size of the meso-level, meso-level size dependence is obtained: the smaller the meso-level size the less brittle the macro-level response becomes (see fig. 5); this meso-level size dependency can be understood as the constitutive behaviour of the material;

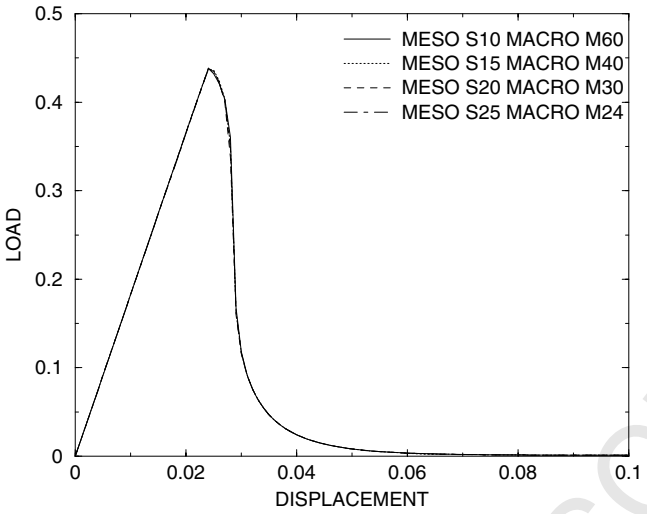

Figure 7: Coupled-volume multi-scale approach: example with homogeneous material

- as a consequence, by linking the size of the macro-level elements to the size of the meso-level, the macro-level element size influence (macro-level mesh dependence) is balanced by different constitutive behaviour coming from different sizes of the meso-level (meso-level size dependence). The macro-level response shows neither macro-level mesh dependency nor meso-level size dependency.

In order to analyse the coupled-volume approach, an example has been performed where the one-dimensional bar with an imperfection on the macro-level has been considered. On the meso-level, however, instead of complex three-phase material, a simplified meso-structure has been used: the material has been described as homogeneous with an imperfection to initiate strain localisation. The results of this coupled-volume multi-scale procedure for the homogeneous material are presented in fig. 7. The macro-level results are clearly unique.

5.2 Meso-level length-scale parameter

The coupled-volume approach is based on abandoning the separation of scales principle and linking a model parameter (size of the meso-level) to a numerical parameter (size of the macro-level mesh element). The next step would be to estimate this model parameter and connect it with some material parameter. The only *material length scale* parameter remaining in the framework of the coupled-volume approach is the meso-level length-scale parameter – the parameter representing the information from the micro-level and responsible for the width of the fracture-process zone on the meso-level.

The influence of this meso-level length-scale parameter on the results of the multi-scale computations has been studied. The same one-dimensional bar as in the previous Section has been analysed. Different length-scale parameters were chosen for the analysis: starting from $\ell = 0.5$ mm, $\ell = 1.0$ mm, $\ell = 2.0$ mm, $\ell = 4.0$ mm and $\ell = 10.0$ mm, and the same macro-level meshes and meso-level size as in Section 3 were used (cf. tabs. 3–4). The results are presented in fig. 8. As it can be seen in fig. 8, with the growth of the meso-level length-scale parameter the results are gradually losing uniqueness: the response remains insensitive to macro-level mesh and meso-level size only for small values of the length-scale parameter ($\ell = 0.5$mm and $\ell = 1$mm). Next (fig. 8–centre left), $\ell = 2$mm is a transition value. In the first stage of the post-peak behaviour the mesh-dependence is observed since the width of the fracture-process zone extends over the meso-cell size, however later on deformation localises further and mesh-objectivity is again found. This trend is even more pronounced for larger length-scales. Thus, starting from the smallest value $\ell = 0.5$mm the length-scale parameter is growing and eventually reaching and even exceeding the size of the tested sample size on the meso-level. However, bearing in mind that the meso-level length-scale carries the information from the micro-level and represents the fracture-process zone on the meso-level, it is obvious that the meso-level sample size should be considerably larger than the length-scale parameter in order to produce insensitive and reliable results on the macro-level. This last expression

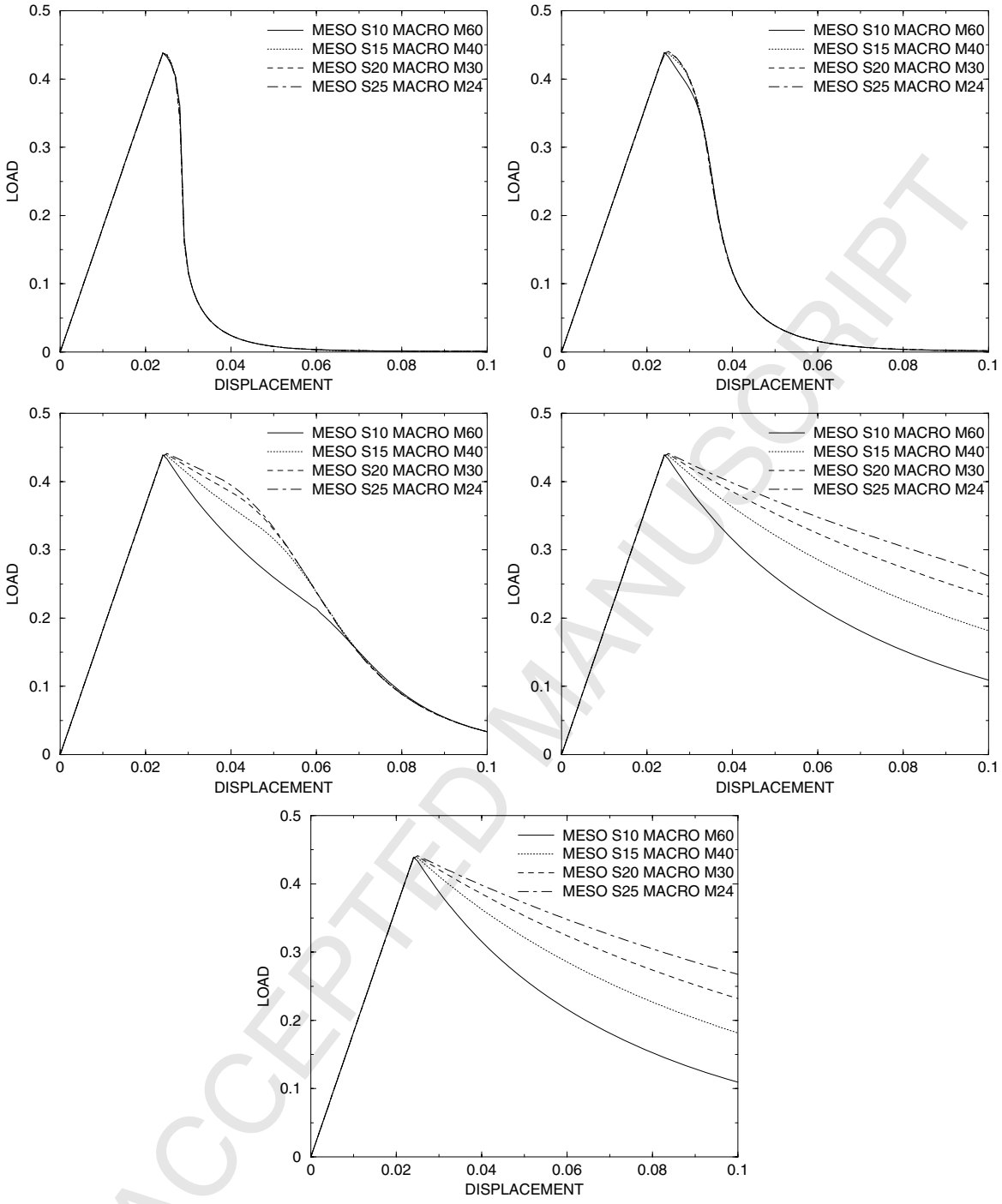

Figure 8: Meso-level length-scale parameter influence on the coupled-volume approach: $\ell = 0.5$ mm (top left), $\ell = 1.0$ mm (top right), $\ell = 2.0$ mm (centre left), $\ell = 4.0$ mm (centre right), $\ell = 10.0$ mm (bottom)

together with evidence in fig. 8 allows to make an estimation of the minimum size of the meso-level and consequently of the minimum mesh size on the macro-level. Both depend on the meso-level length-scale as

$$L_{\mathrm{M}} > 10\ell \tag{29}$$

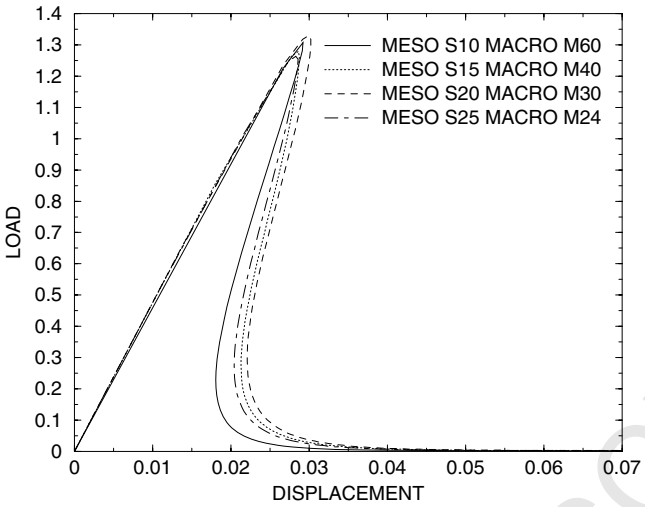

Figure 9: Coupled-volume multi-scale approach: volume fraction of inclusions 30%

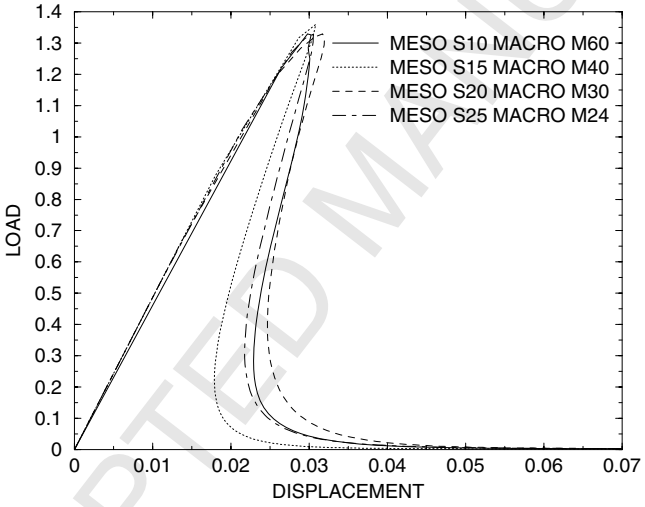

Figure 10: Coupled-volume multi-scale approach: volume fraction of inclusions 45%

Here, L_{M} represents the macro-level mesh size. Once the size of the macro-level mesh (and the corresponding meso-level sample size) is verified according to the meso-level length scale, the coupled-volume multi-scale procedure is fully defined. Two further restrictions are that the meso-level length scale is coupled to the finite element size on the meso-level and the macro-level mesh size L_{M} should be chosen such that the response on macro-level should be described accurate enough.

5.3 Multi-phase meso-structure

The results of the coupled-volume multi-scale framework for a three-phase material on the meso-level with different volume fractions of inclusions are presented in figs. 9, 10 and 11. Again it can be seen, that both macro-level mesh sensitivity and meso-level size sensitivity are solved simultaneously. The difference in load-displacement diagrams, appearing in figs. 9, 10 and 11 can be explained by statistical effects: the locations of inclusions in different meso-level samples are responsible for this small deviation of results. However, with increasing the size of the unit cell the deviation

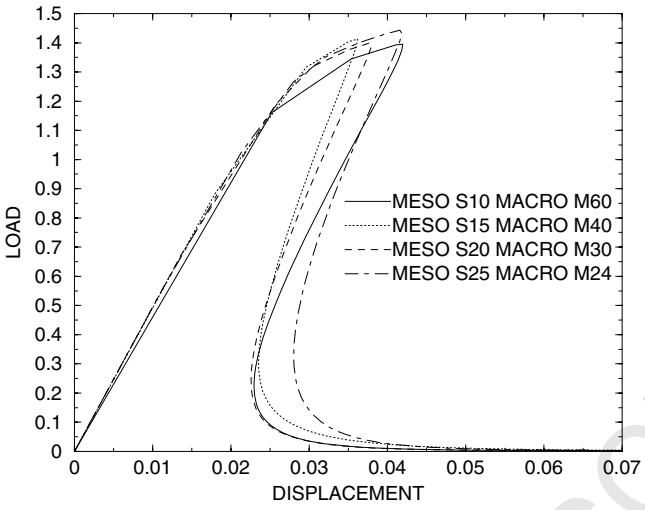

Figure 11: Coupled-volume multi-scale approach: volume fraction of inclusions 60%

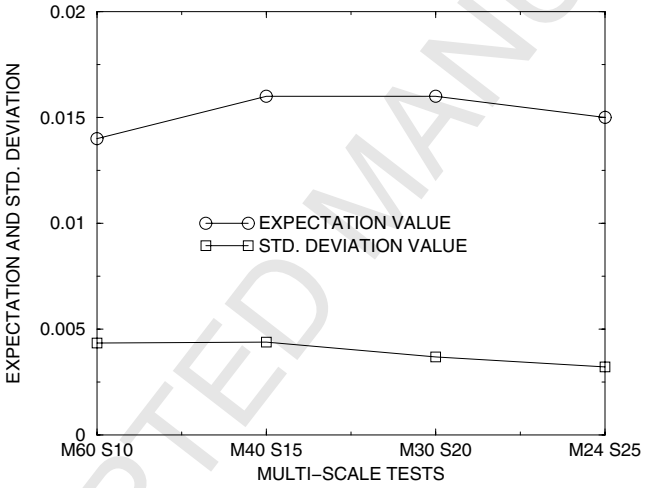

Figure 12: Expectation and standard deviation values of the dissipated energy for different coupled-volume multi-scale analysis (volume fraction of inclusions 30%)

of the results is decreasing. Thus, the conclusion can be made that the macro-level response sensitivity to the particular meso-level realisation will decrease with increasing the size of the meso-level. This last statement has been verified on the basis of the statistical analysis of the coupled-volume multi-scale results: five different realisations of the meso-level unit cells for each meso-level size have been considered. Corresponding macro-level responses have been obtained in terms of dissipated energy. Then the statistical analysis based on the mathematical expectation and standard deviation has been performed. The result is presented in fig. 12. It can be seen from fig. 12, that with increasing the size of the meso-level (i.e. increasing the size of the macro-level element) the mathematical expectation of the dissipated energy remains relatively constant. Also the value of the standard deviation is slightly decreasing for bigger sizes. Thus, no conclusion can be drawn from the statistical point of view on what should be the size of the macro-level element size and the corresponding meso-level cell size. In order to select macro-level element size and meso-level cell size, one should consider eq. (29). Furthermore, snap-back behaviour may occur on the meso-level in case the meso-level cell size is too large. Since snap-back on the meso-level implies that a macro-level strain cannot be uniquely related to a macro-level stress, the use of too

large meso-level cells should be avoided.

Note 7 *The results in figs. 9–11 have been generated by using one value for the length-scale, namely $\ell = 0.63$ mm. In the discussion of fig. 8 it was established that the macro-level ductility is set by the length-scale present on the meso-level. Thus, the ductility of the results in figs. 9–11 can be manipulated by varying the mesoscopic length-scale.*

Note 8 *As a validation test, the results of figs. 9–11 should be compared with a simulation whereby the entire specimen is modelled as a heterogeneous material on the macro-level. Although unfortunately such results are at present not available for the considered problem, nevertheless attention is drawn to the work of [Kouznetsova, 2002], who analysed a specimen with a periodic arrangement of circular holes. The applied modelling approaches were a multi-scale method as well as a detailed macro-level modelling. A moderate amount of softening was observed on meso-level and macro-level, which was caused by the geometric nonlinearities. A good agreement between the two sets of results was found for the case where the macro-level element size coincided with the meso-level cell size. For further study of this issue, the following aspects may be considered:*

- *If the macro-level is modelled as a heterogeneous structure, a single meso-cell can be taken and copied periodically, or alternatively a fully random distribution of particles may be taken. This could serve as yet another test whether the selected size of the meso-cell is appropriate.*
- *Similarly, such a test may serve as a validation of the periodic boundary conditions that are used on the meso-level.*

A detailed analysis of the material evolution for the macro-level mesh "MACRO M40" and meso-level size "MESO S15" is described below. For this test the volume fractions of inclusions equals 45 %; the finite element discretisation is similar to that shown in fig. 3.

Overall remarks. Figs. 13–18 are built up in the following way:

- several (6) steps are presented in these figures, corresponding to different loading regimes: figs. 13–15 correspond to the pre-peak regimes, figs. 16–18 to the post-peak or softening behaviour; it should be emphasized, that the pre-peak non-linear response is a natural outcome of the coupled-volume multi-scale modelling technique; the pre-peak nonlinear response is also observed in experiments;
- at the top of all figures the global macro-level response in the form of load-displacement curve is presented;
- the meso-level behaviour is analysed for the elements outside the imperfection (fig. 13–18–left) and inside the imperfection (fig. 13–18–right), thus two sets of figures are needed. *Note, that the global macro-level response is similar for both sets*;
- the meso-level responses are represented by means of the contour plots of equivalent strains (the middle picture) and the load-displacement curves (the bottom picture).

Thus, analysing all figures correspondingly the following observations can be made:

Pre-peak regime. It can be seen from the top picture of fig. 13 that the macro-level is in the linear-elastic regime. Corresponding to this macro-linear-elastic point, two meso-level elements outside (lower parts of fig. 13–left) and inside the imperfection zone (lower parts of fig. 13–right) also experience linear elastic behaviour. For both outside and inside meso-level elements the contour plots (the middle pictures in figs. 13–left and 13–right) look more or less similar, the small difference is dictated only by the different width of the corresponding macro-level elements: the width of the imperfection is 0.9 times the width of the rest of the bar. This difference in the macro-level element width influences the value of the strain field in the particular macro integration points: the strains in the element with imperfection are somewhat higher than in the element without imperfection. And this difference in the strain field, in turn, slightly changes the boundary condition on the meso-level. This slight difference is also noticeable in the load-displacement curves (the bottom pictures in figs. 13–left and 13–right). Nevertheless, both meso-level elements outside the imperfection and inside the imperfection are still in the linear-elastic regime. All three components of the meso-level heterogeneous material are linear elastic.

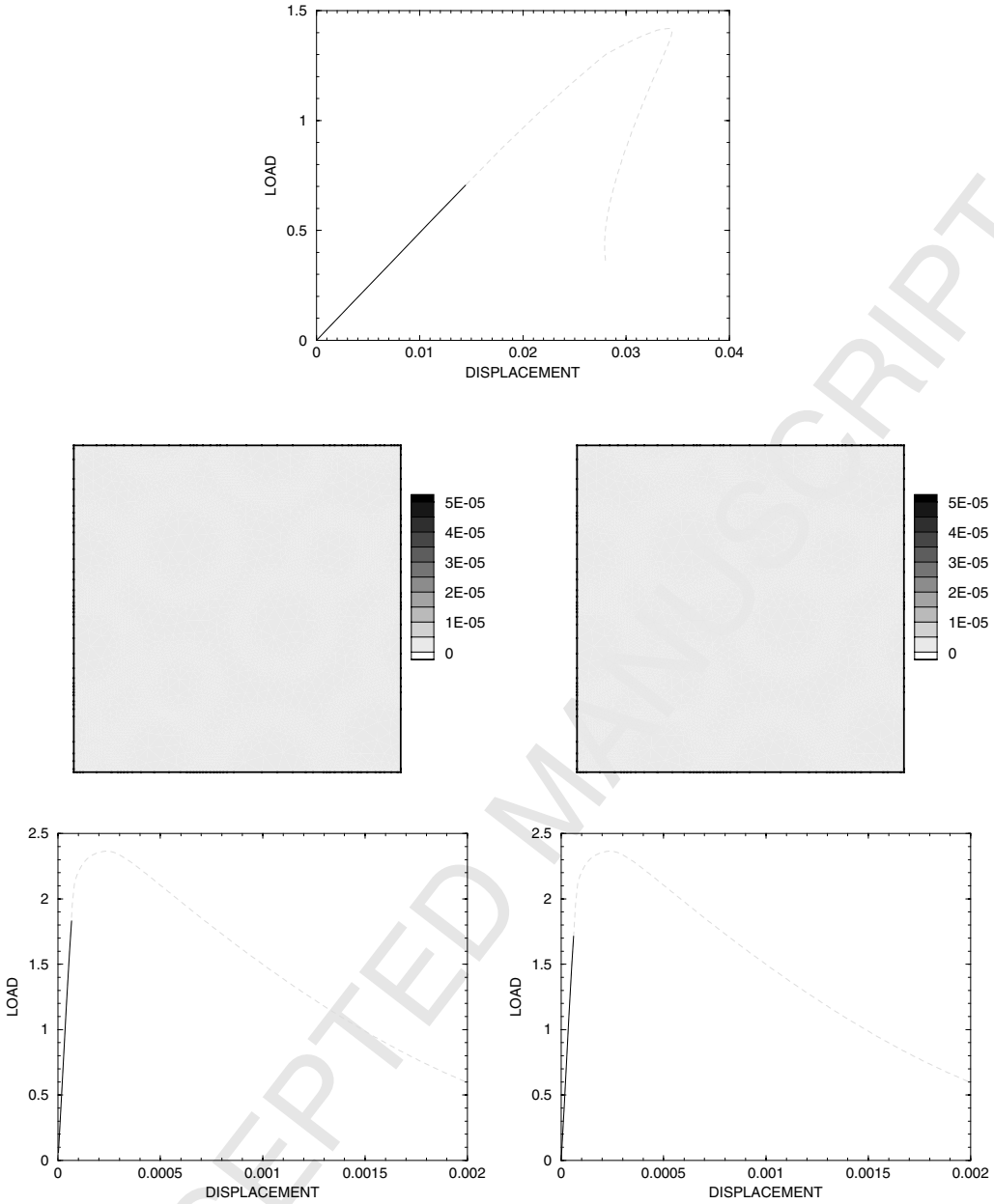

Figure 13: Multi-scale evolution. Top to bottom: macro-level response in the form of load-displacement curve, meso-level contour and the load-displacement curve of the element outside the imperfection (left) and inside the imperfection (right) in the linear-elastic regime.

The picture changes in fig. 14. Here, as it can be seen from the load-displacement curve of the macro-level response (top of the figures), the macro-level starts experiencing the initiation of damage. The difference in the corresponding meso-level elements is larger. Now the equivalent strain in the interfacial transition zones of both inside and outside the imperfection has exceeded the critical value and started to soften causing the pre-peak damage on the global meso response (the bottom pictures in figs. 14–left and 14–right): more on the meso-element inside imperfection and less outside. Still no localisation can be seen in the contour plots (the middle pictures in figs. 14–left and 14–right).

As the macro-level response approaches to the peak (the top of fig. 15), the meso-level response starts being quali-

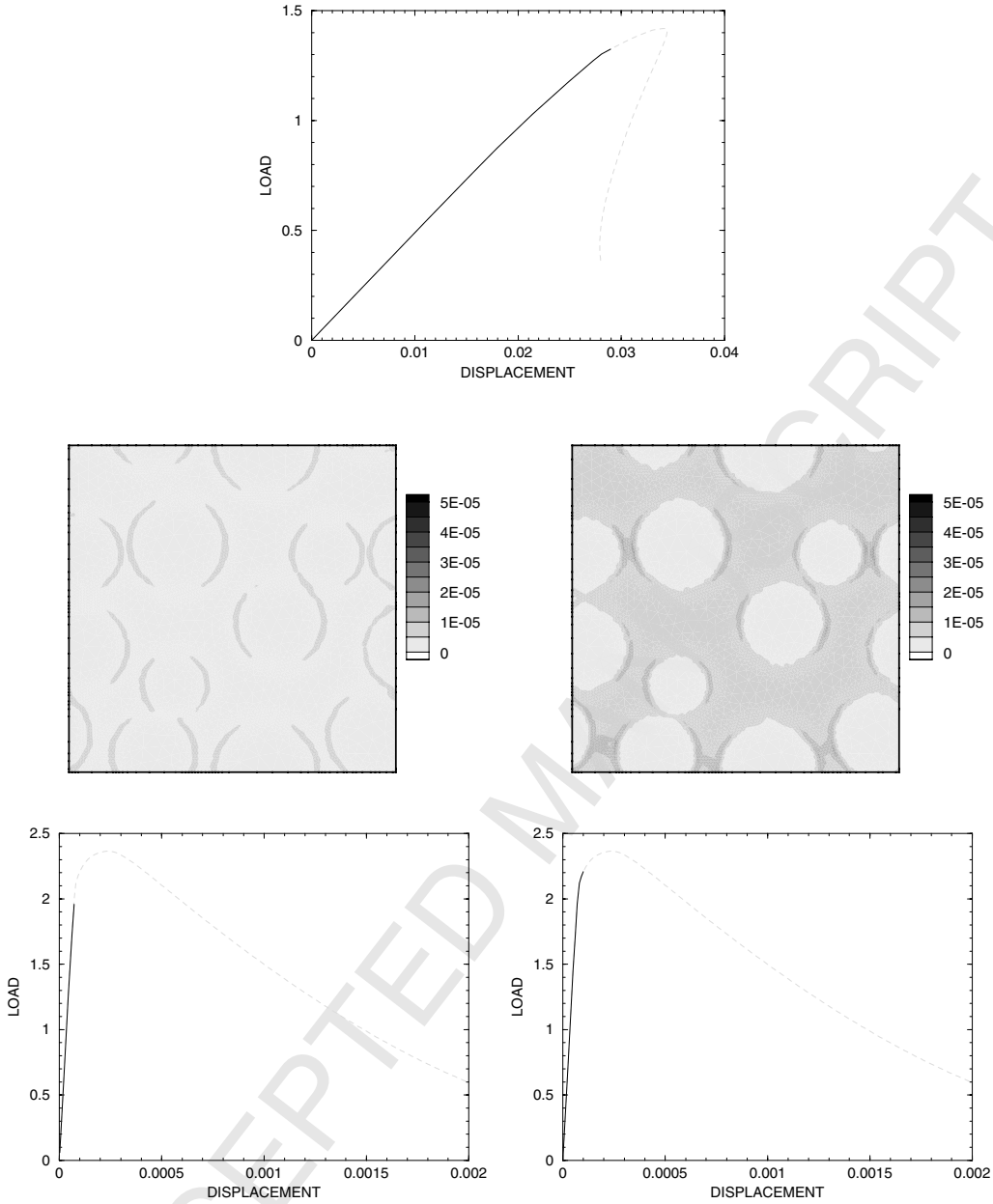

Figure 14: Multi-scale evolution. Top to bottom: macro-level response in the form of load-displacement curve, meso-level contour and the load-displacement curve of the element outside the imperfection (left) and inside the imperfection (right) in nonlinear pre-peak regime.

tatively different for elements inside and outside the imperfection. The pre-peak regime can be characterised by the first indication of the dominant crack in the meso-element inside the imperfection (the middle of fig. 15–right), the global meso-level load-displacement response shows *just before the peak* behaviour (the bottom of fig. 15–right). The meso-element outside the imperfection is still in the loading process and it is still in the ascending branch (the middle / bottom of fig. 15–left).

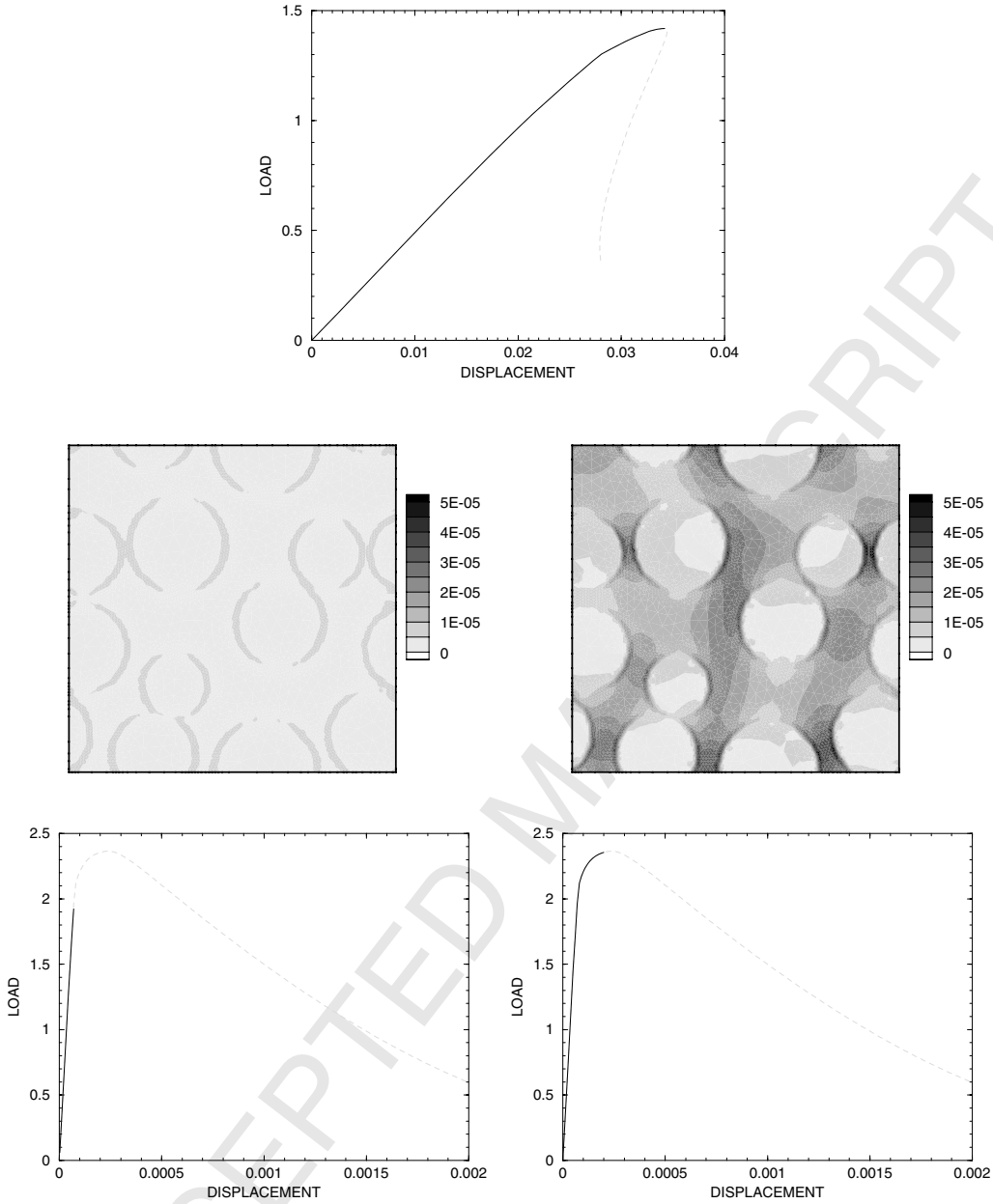

Figure 15: Multi-scale evolution. Top to bottom: macro-level response in the form of load-displacement curve, meso-level contour and the load-displacement curve of the element without localisation (left) and with localisation (right) at the peak.

Post-peak regime. Starting from this point the meso-element outside the imperfection is in the unloading regime (the middle / bottom of fig. 16–left). The meso-element inside the imperfection shows the localised region – the dominant crack has appeared (the middle of fig. 16–right) and the load-displacement curve is in softening regime (the bottom of fig. 16–right). As a result of this meso-level localisation, the macro-level load-displacement curve has passed the peak (the top of fig. 16).

The evolution of material behaviour after localisation of deformation in the meso cell is presented in figs. 17-18. The softening regime close to the peak (fig. 17) and the softening regime far from the peak (fig.18) have a similar character: the meso-element inside the imperfection has a clear localisation zone or dominant crack, and the material surrounding

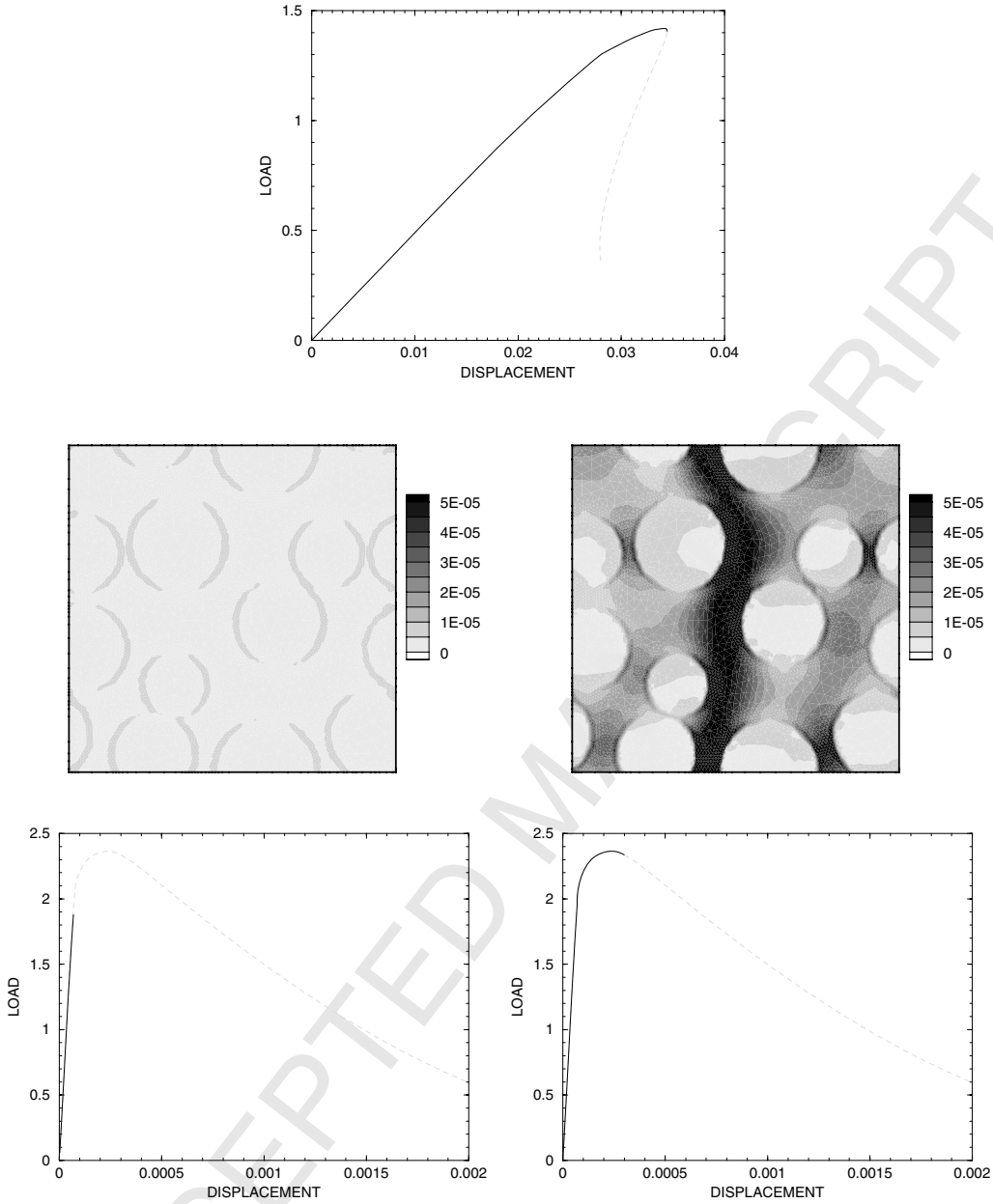

Figure 16: Multi-scale evolution. Top to bottom: macro-level response in the form of load-displacement curve, meso-level contour and the load-displacement curve of the element without localisation (left) and with localisation (right) in the post-peak regime.

the localisation zone is experiencing unloading behaviour. This unloading behaviour further develops (it can be seen on the middle / bottom figs. 17–right) and eventually the meso-level element is fully damaged (the middle of fig. 18–right). The meso-element outside the imperfection also experiences unloading (figs. 17-18–left).

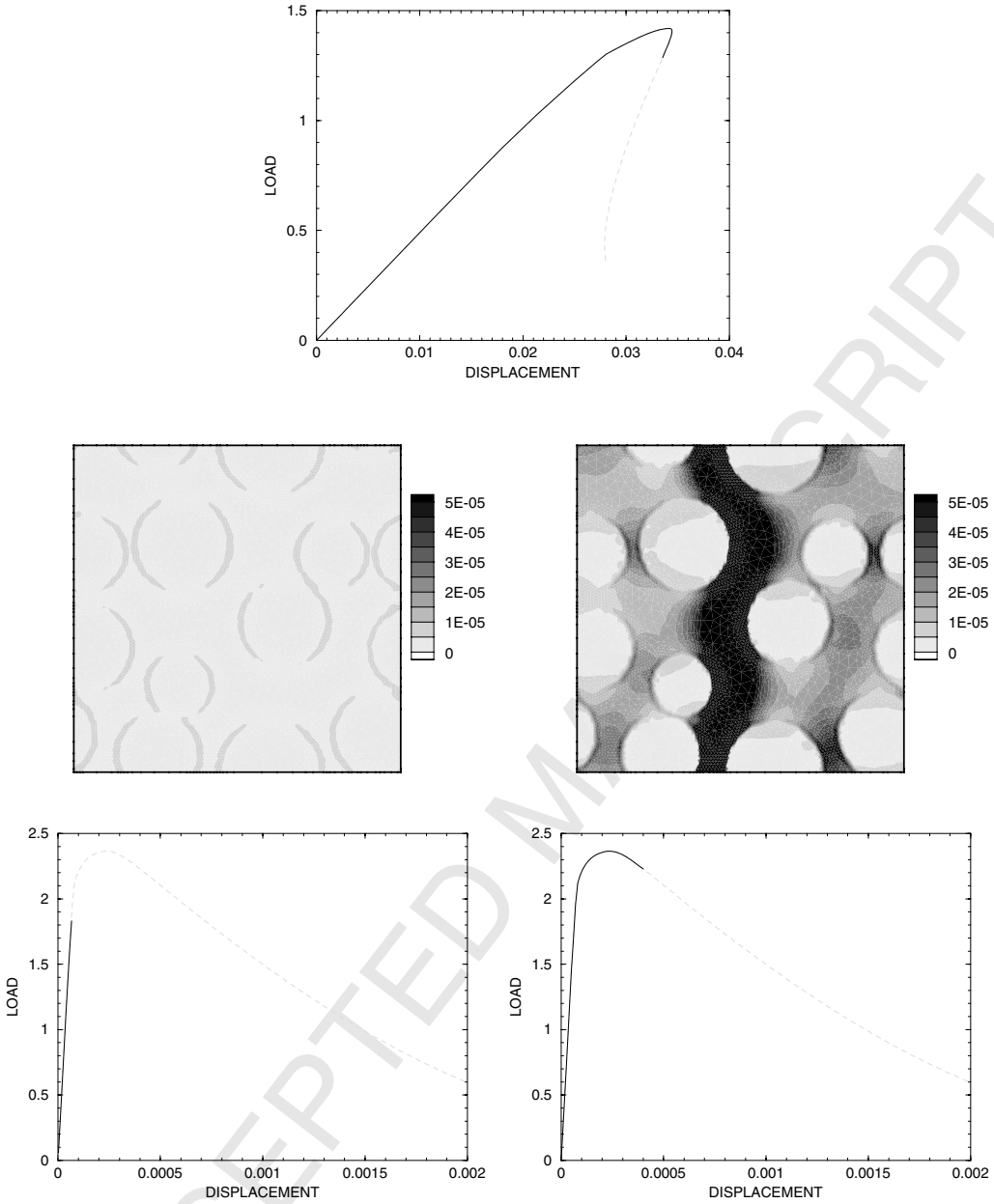

Figure 17: Multi-scale evolution. Top to bottom: macro-level response in the form of load-displacement curve, meso-level contour and the load-displacement curve of the element without localisation (left) and with localisation (right) in the softening regime close to the peak.

6 Conclusions

Attention in this paper has been given to the computational homogenisation technique in the framework of the multi-scale model. As an example, the behaviour of a one-dimensional bar with an imperfection has been analysed. The meso-level has been described as a three-phase material with stiff inclusions, embedded in a softer matrix and surrounded by an interfacial transition zone. The global response has been analysed with respect to a macro-level discretisation parameter (macro-level mesh dependence) and a meso-level model parameter (meso-level size dependence).

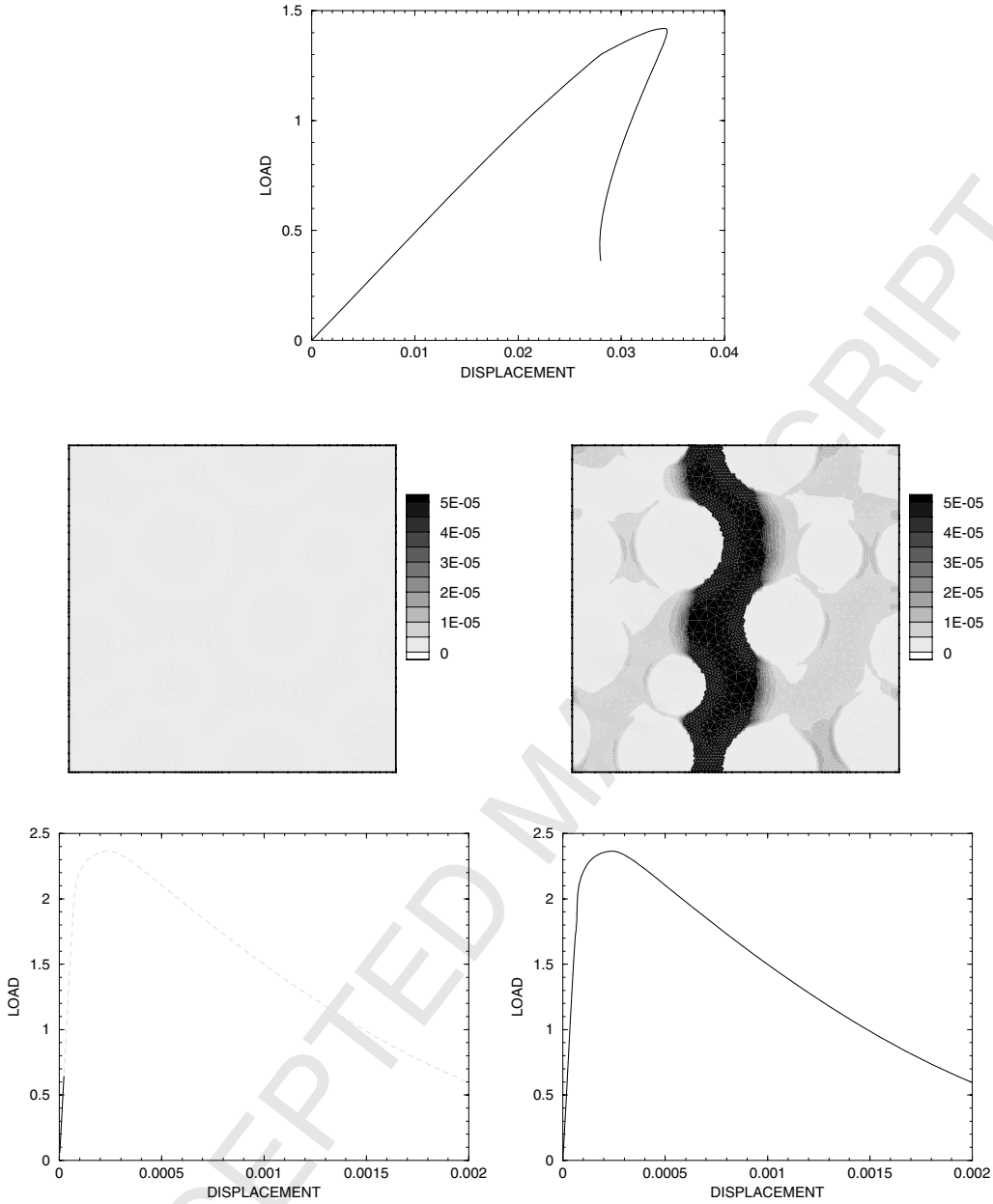

Figure 18: Multi-scale evolution. Top to bottom: macro-level response in the form of load-displacement curve, meso-level contour and the load-displacement curve of the element without localisation (left) and with localisation (right) in the fully damaged regime.

A distinction between local and non-local numerical schemes has been made. The local multi-scale model has been analysed first. Again pre- and post-peak regimes were considered. In the pre-peak regime the macro-level response shows no signs of macro-level mesh dependency nor meso-level size dependency. This last observation supports the conclusion obtained earlier that an RVE exists in this regime [Gitman, 2006, Gitman et al., 2007c]. On the contrary, in the post-peak regime the results show a strong macro-level mesh dependency and meso-level size dependency, which in turn supports the conclusion of an RVE non-existence in this regime. No ”representative” size can be found, thus with increasing the size the material behaves differently – this explains meso-level size dependency of the multi-scale results.

The dependency of the multi-scale results on the macro-level mesh size can be overcome by introducing a non-local multi-scale scheme, for example a gradient enhanced framework such as the second-order homogenisation scheme. Unfortunately, this type of models also have disadvantages. Firstly, the implementation is relatively complicated. Secondly and more importantly, the dependence on the meso-level sample size is not accounted for.

A multi-scale model is desired that can describe the behaviour of a material with a composite structure based on the computational homogenisation but being independent of the macro-level mesh and meso-level size. Such a model has been introduced as the *coupled-volume* approach. The key idea is that the size of the meso-level sample should be identical to the size of the macro-level integration volume that is associated with this meso-level sample. This unique link of macro-level mesh size and meso-level sample size abandons the concept of separation of scales, which was present in the local model and previous non-local models. Since this approach does not rely upon the existence of an RVE, it can also be used in softening. With the coupled-volume approach results can be obtained that do not depend on the macro-level mesh size nor the meso-level sample size. Thus, the conclusion can be drawn that the coupled-volume multi-scale model is an objective tool to describe the multi-scale behaviour of the composite material.

References

[Askes and Metrikine, 2002] Askes, H. and Metrikine, A. (2002). One-dimensional dynamically consistent gradient elasticity models derived from a discrete microstructure. Part 2: Static and dynamic response. *European Journal of Mechanics A/Solids*, 21:573–588.

[Askes and Metrikine, 2005] Askes, H. and Metrikine, A. (2005). Higher-order continua derived from discrete media: continualisation aspects and boundary conditions. *International Journal of Solids and Structures*, 42:187–202.

[Bažant, 1991] Bažant, Z. (1991). Why continuum damage is nonlocal: micromechanics arguments. *Journal of Engineering Mechanics*, 117:1070–1087.

[Bažant and Jirásek, 1994] Bažant, Z. and Jirásek, M. (1994). Damage nonlocality due to microcrack interactions: statistical determination of crack influence function. In Bažant, Z., Bittnar, Z., Jirásek, M., and Mazars, J., editors, *Fracture and damage in quasibrittle structures*. E& FN Spon.

[Bažant and Oh, 1983] Bažant, Z. and Oh, B. (1983). Crack band theory for fracture of concrete. *Materials and Structures. RILEM*, 16:155–177.

[Bažant and Pijaudier-Cabot, 1989] Bažant, Z. and Pijaudier-Cabot, G. (1989). Measurement of characteristic length of nonlocal continuum. *Journal of Engineering Mechanics*, 115(4):755–767.

[Ben Dhia, 2006] Ben Dhia, H. (2006). Global-local approaches: the Arlequin Method. *European Journal of Computational Mechanics*, 15:67–80.

[Ben Dhia and Rateau, 2005] Ben Dhia, H. and Rateau, G. (2005). The Arlequin method as a flexible engineering design tool. *International Journal for Numerical Methods in Engineering*, 62:1442–1462.

[Breuls et al., 2002] Breuls, R., Sengers, B., Oomens, C., and Bouten, C. (2002). Predicting local cell deformations in engineered tissue constructs: A multilevel finite element approach. *ASME Journal of Biomechanical Engineering*, 124:198–207.

[Chang and Gao, 1995] Chang, C. and Gao, J. (1995). Second-gradient constitutive theory for granular material with random packing structure. *International Journal of Solids and Structures*, 32:2279–2293.

[de Borst, 1987] de Borst, R. (1987). Computation of post-bifurcation and post-failure behaviour of strain-softening solids. *Computers & Structures*, 25:211–224.

[Fatemi et al., 2003] Fatemi, J., Onck, P., Poort, G., and Keulen, F. V. (2003). Cosserat moduli of anisotropic cancellous bone: A micromechanical analysis. *Journal de Physique IV*, 105:273–280.

[Feyel and Chaboche, 2000] Feyel, F. and Chaboche, J. (2000). FE^2 multiscale approach for modelling the elastoplastic behaviour of long fibre sic/ti composite materials. *Computer Methods in Applied Mechanics and Engineering*, 183:309–330.

[Ghosh et al., 2001] Ghosh, S., Lee, K., and Raghavan, P. (2001). A multi-level computational model for multi-scale damage analysis in composite and porous materials. *International Journal of Solids and Structures*, 38:2335–2385.

[Gitman, 2006] Gitman, I. (2006). *Representative volumes and multi-scale modelling of quasi-brittle materials*. PhD thesis, Delft University of Technology. Available from http://www.library.tudelft.nl/.

[Gitman et al., 2005] Gitman, I., Askes, H., and Aifantis, E. (2005). The representative volume size in static and dynamic micro-macro transitions. *International Journal of Fracture*, 135:L3–L9.

[Gitman et al., 2007a] Gitman, I., Askes, H., and Aifantis, E. (2007a). Gradient elasticity with internal length and internal inertia based on the homogenisation of a representatve volume element. *Journal of the Mechanical Behavior of Materials*, 18:1–16.

[Gitman et al., 2007b] Gitman, I., Askes, H., and Sluys, L. (2007b). A coupled-volume approach to the multi-scale modelling of quasi-brittle materials. *Materials Science Forum*, 539–543:2582–2587.

[Gitman et al., 2007c] Gitman, I., Askes, H., and Sluys, L. (2007c). Representative volume: existence and size determination. *Engineering Fracture Mechanics*, 74:2518–2534.

[Gitman et al., 2006] Gitman, I., Gitman, M., and Askes, H. (2006). Quantification of stochastically stable representative volumes for random heterogeneous materials. *Archive of Applied Mechanics*, 75:79–92.

[Guedes and Kikuchi, 1990] Guedes, J. and Kikuchi, N. (1990). Preprocessing and postprocessing for materials based on the homogenization method with adaptive finite element methods. *Computer Methods in Applied Mechanics and Engineering*, 83:143–198.

[Gutiérrez, 2004] Gutiérrez, M. (2004). Energy release control for numerical simulations of failure in quasi-brittle solids. *Communications in Numerical Methods in Engineering*, 20:19–29.

[Hill, 1963] Hill, R. (1963). Elastic properties of reinforced solids: some theoretical principles. *Journal of the Mechanics and Physics of Solids*, 11:357–372.

[Hill, 1967] Hill, R. (1967). The essential structure of constitutive laws for metal composites and polycristals. *Journal of the Mechanics and Physics of Solids*, 15:79–95.

[Hill, 1984] Hill, R. (1984). On macroscopic effects of heterogeneity in elastoplastic media at finite strain. *Mathematical Proceedings of the Cambridge Philosophical Society*, 95:481–494.

[Kanit et al., 2003] Kanit, T., Forest, S., Galliet, I., Mounoury, V., and Jeulin, D. (2003). Determination of the size of the representative volume element for random composites: statistical and numerical approach. *International Journal of Solids and Structures*, 40:3647–3679.

[Kouznetsova, 2002] Kouznetsova, V. (2002). *Computational homogenization for the multi-scale analysis of multi-phase materials*. PhD thesis, Technical University Eindhoven. Available from http://www.mate.tue.nl.

[Kouznetsova et al., 2001] Kouznetsova, V., Brekelmans, W., and Baaijens, F. (2001). An approach to micro-macro modeling of heterogeneous materials. *Computational Mechanics*, 27:37–48.

[Kouznetsova et al., 2002] Kouznetsova, V., Geers, M., and Brekelmans, W. (2002). Multi-scale constitutive modelling of heterogeneous materials with a gradient-enhanced computational homogenization scheme. *International Journal for Numerical Methods in Engineering*, 54:1235.

[Lee and Ghosh, 1995] Lee, K. and Ghosh, S. (1995). Multiple scale analysis of heterogeneous elastic structures using homogenization theory and Voronoi cell finite element method. *International Journal of Solids and Structures*, 32:27–62.

[Lee and Ghosh, 1996] Lee, K. and Ghosh, S. (1996). Small deformation multi-scale analysis of heterogeneous materials with the Voronoi cell finite element model and homogenization theory. *Computational Materials Science*, 7:131–146.

[Lemaitre and Chaboche, 1990] Lemaitre, J. and Chaboche, J.-L. (1990). *Mechanics of solid materials*. Cambridge University Press, Cambridge.

[Markovic and Ibrahimbegovic, 2004] Markovic, D. and Ibrahimbegovic, A. (2004). On micro-macro interface conditions for micro scale based FEM for inelastic behaviour of heterogeneous materials. *Computer Methods in Applied Mechanics and Engineering*, 193:5503–5523.

[Massart, 2003] Massart, T. (2003). *Multi-scale modeling of damage in masonry structures*. PhD thesis, Technical University Eindhoven. Available from http://www.mate.tue.nl.

[Metrikine and Askes, 2002] Metrikine, A. and Askes, H. (2002). One-dimensional dynamically consistent gradient elasticity models derived from a discrete microstructure. Part 1: Generic formulation. *European Journal of Mechanics A/Solids*, 21:555–572.

[Michel et al., 1999] Michel, J., Moulinec, H., and Suquet, P. (1999). Effective properties of composite materials with periodic microstructure: a computational approach. *Computer Methods in Applied Mechanics and Engineering*, 16:109–143.

[Miehe et al., 1999] Miehe, C., Schotte, J., and Schröder, J. (1999). Computational micro-macro transitions and overall moduli in the analysis of polycrystals at large strains. *Computational Materials Science*, 16:372–382.

[Mühlhaus and Oka, 1996] Mühlhaus, H.-B. and Oka, F. (1996). Dispersion and wave propagation in discrete and continuous models for granular materials. *International Journal of Solids and Structures*, 33:2841–2858.

[Nemat-Nasser and Hori, 1999] Nemat-Nasser, S. and Hori, M. (1999). *Micromechanics: overall properties of heterogeneous materials*. Elsevier.

[Peerlings, 1999] Peerlings, R. (1999). *Enhanced damage modelling for fracture and fatigue*. PhD thesis, Technical University Eindhoven. Available from http://www.mate.tue.nl.

[Peerlings and Fleck, 2004] Peerlings, R. and Fleck, N. (2004). Computational evaluation of strain gradient elasticity constants. *International Journal for Multiscale Computational Engineering*, 2:599–619.

[Pijaudier-Cabot, 1995] Pijaudier-Cabot, G. (1995). Non local damage. In Mühlhaus, H.-B., editor, *Continuum models for materials with microstructure*. John Wiley & Sons Ltd.

[Pijaudier-Cabot and Bažant, 1987] Pijaudier-Cabot, G. and Bažant, Z. (1987). Nonlocal damage theory. *Journal of Engineering Mechanics*, 113:1512–1533.

[Ru and Aifantis, 1993] Ru, C. and Aifantis, E. (1993). A simple approach to solve boundary-value problems in gradient elasticity. *Acta Mechanica*, 101:59–68.

[Simone, 2003] Simone, A. (2003). *Continuous-discontinuous modelling of failure*. PhD thesis, Delft University of Technology. Available from http://www.library.tudelft.nl/.

[Smit et al., 1998] Smit, R., Brekelmans, W., and Meijer, H. (1998). Prediction of the mechanical behavior of nonlinear heterogeneous systems by multi-level finite element modeling. *Computer Method in Applied Mechanics and Engineering*, 55:181–192.

[Suiker et al., 2001] Suiker, A., de Borst, R., and Chang, C. (2001). Micro-mechanical modelling of granular material. Part 1: derivation of a second gradient micro-polar constitutive theory. *Acta Mechanica*, 149:161–180.

[Terada and Kikuchi, 2001] Terada, K. and Kikuchi, N. (2001). A class of general algorithms for multi-scale analyses of heterogeneous media. *Computer Methods in Applied Mechanics and Engineering*, 190:5427–5464.

[Trukozko and Zijl, 2002] Trukozko, A. and Zijl, W. (2002). Complementary finite element methods applied to the numerical homogenization of 3d absolute permeability. *Communications in Numerical Methods in Engineering*, 18:31–41.

[van der Sluis, 2001] van der Sluis, O. (2001). *Homogenisation of structured elastoviscoplastic solids*. PhD thesis, Technical University Eindhoven. Available from http://www.mate.tue.nl.

[Wang and Sun, 2002] Wang, Z.-P. and Sun, C. (2002). Modeling micro-inertia in heterogeneous materials under dynamic loading. *Wave Motion*, 36:473–485.

[Zimmermann et al., 2003] Zimmermann, S., Kleinman, C., and Hordijk, D. (2003). Multi-scale modeling of concrete-like composites. In *9th International conference of the mechanical behaviour of materials*.

[Zohdi et al., 2001] Zohdi, T., Wriggers, P., and Huet, C. (2001). A method of substructuring large-scale computational micromechanical problems. *Computer Methods in Applied Mechanics and Engineering*, 190:5639–5656.